AD NUMBER

AD808700

LIMITATION CHANGES

TO:

Approved for public release; distribution is unlimited.

FROM:

**Distribution authorized to U.S. Gov't. agencies and their contractors;
Administrative/Operational Use; MAR 1967. Other requests shall be referred to Arnold Engineering Development Center, Arnold AFB, TN.**

AUTHORITY

AEDC ltr dtd 15 Nar 1973

AEDC-TR-67-33

BUFFET RESPONSE OF AEROELASTICALLY SCALED TITAN III MISSILE CONFIGURATIONS AT TRANSONIC MACH NUMBERS

J. E. Robertson and T. R. Brice

ARO, Inc.

March 1967

PROPULSION WIND TUNNEL FACILITY
ARNOLD ENGINEERING DEVELOPMENT CENTER
AIR FORCE SYSTEMS COMMAND
ARNOLD AIR FORCE STATION, TENNESSEE

NOTICES

When U. S. Government drawings specifications, or other data are used for any purpose other than a definitely related Government procurement operation, the Government thereby incurs no responsibility nor any obligation whatsoever, and the fact that the Government may have formulated, furnished, or in any way supplied the said drawings, specifications, or other data, is not to be regarded by implication or otherwise, or in any manner licensing the holder or any other person or corporation, or conveying any rights or permission to manufacture, use, or sell any patented invention that may in any way be related thereto

Qualified users may obtain copies of this report from the Defense Documentation Center.

References to named commercial products in this report are not to be considered in any sense as an endorsement of the product by the United States Air Force or the Government.

BUFFET RESPONSE OF AEROELASTICALLY SCALED TITAN III MISSILE CONFIGURATIONS AT TRANSONIC MACH NUMBERS

J. E. Robertson and T. R. Brice
ARO, Inc.

AF - AEDC
Arnold AFS Tenn

FOREWORD

The work reported herein was done at the request of the Space Systems Division (SSD), Air Force Systems Command (AFSC), for the Aerospace Division of the Martin-Marietta Corporation under Program Element 64409094, System 624A.

The test results presented were obtained by ARO, Inc. (a subsidiary of Sverdrup & Parcel and Associates, Inc.), contract operator of the Arnold Engineering Development Center (AEDC), AFSC, Arnold Air Force Station, Tennessee, under Contract AF40(600)-1200. The test was conducted under ARO Project No. PB0605 from January 18 through 27, 1966, March 14 through 16, 1966, May 2 through 18, 1966, and October 31 through November 10, 1966. The manuscript was submitted for publication on January 27, 1967.

Information in this report is embargoed under the Department of State International Traffic in Arms Regulations. This report may be released to foreign governments by departments or agencies of the U. S. Government subject to approval of the Space Systems Division (SSBDD), Los Angeles, California, or higher authority. Private individuals or firms require a Department of State export license.

This technical report has been reviewed and is approved.

Richard W. Bradley
Lt Col, USAF
AF Representative, PWT
Directorate of Test

Leonard T. Glaser
Colonel, USAF
Director of Test

ABSTRACT

A wind tunnel investigation was conducted to obtain the structural response of 0.07-scaled aeroelastic models of Titan III missile configurations to buffet airloads at transonic Mach numbers. Test results in the form of bending-moment response in the pitch and yaw planes were obtained for various payload, upper stage, and booster combinations. The tests were conducted in the Mach number range from 0.6 to 1.4 and at angles of attack ranging from 0 to 4 deg. The basic Centaur/Voyager configuration experienced flutter in the first pitch and yaw elastic bending modes as Mach number was increased above 0.80. The flutter was eliminated by (1) adding to the payload a cylindrical shroud having the same diameter as the payload and (2) adding to the payload a boattail shroud with a ring of vortex generators upstream of the boattail. The MOL and Apollo configurations exhibited slightly different trends in the bending-moment variations with Mach number, although both configuration families experienced peak loads at Mach numbers near 0.95. Increasing dynamic pressure caused a proportionate increase in the pitch and yaw structural response. Increasing angle of attack, in general, resulted in a reduction in the structural response, although there were deviations from this trend for certain configurations.

CONTENTS

APPENDIXES

NOMENCLATURE

C_A	Aerodynamic damping, $\frac{\text{lb-sec}}{\text{ft}}$
C_c	Control-system damping, $\frac{\text{lb-sec}}{\text{ft}}$
C_s	Structural damping, $\frac{\text{lb-sec}}{\text{ft}}$
d	Model core diameter, ft
F_N	Normal force on support springs, lb
F_Y	Side force on support springs, lb
M_∞	Free-stream Mach number
MS	Model station, in.
p_∞	Free-stream static pressure, psf
q_∞	Free-stream dynamic pressure $0.7\, p_\infty M_\infty^2$, psf
q'_∞	Free-stream dynamic pressure for off-normal test conditions, psf
Re_d	Reynolds number based on model core diameter, $(V_\infty d)/\nu_\infty$
V_∞	Free-stream velocity, ft/sec
W	Total model weight, lb
α	Angle of attack, deg
ν_∞	Kinematic viscosity of the free stream, ft^2/sec
σ_M	Total elastic rms bending moment, in.-lb
σ'_M	Total elastic rms bending moment for test conditions at off-normal dynamic pressures, in.-lb
σ_{MT}	Total rms bending moment, in.-lb
ϕ	Angular coordinate about the model, positive clockwise looking upstream with $\phi = 0$ at the top of the model, deg

PHASE II TEST CONFIGURATIONS

Configuration Number	Configuration Description
1	Titan III-A, Transtage/Std 1100-lb fairing, 5-segment SRM's
2	Titan III-C, Transtage/Std 21,000-lb fairing, 5-segment SRM's
3	Titan III-C, Centaur/Voyager, 5-segment SRM's
4	Titan III-C, Centaur/Voyager with Shroud A, 5-segment SRM's
5	Titan III-C, Centaur/Voyager with Shroud B, 5-segment SRM's
6	Titan III-C, Centaur/Voyager with Shroud C, 5-segment SRM's
8	Titan III-C, Centaur/Voyager with Shroud B, 7-segment SRM's
9	Titan III-C, Transtage/15-ft-diam Bulbous Payload, 5-segment SRM's
15	Titan III-C, Centaur/Voyager with large forward vortex generators, 5-segment SRM's
16	Titan III-C, Centaur/Voyager with aft vortex generators, 5-segment SRM's
17	Titan III-C, Centaur/Voyager with splitter plates, 5-segment SRM's
19	Titan III-C, Transtage, 13-ft-diam, 20-ft-long Cylinder/Blunted Cone, 5-segment SRM's
20	Titan III-C, Transtage, 13-ft-diam, 40-ft-long Cylinder/Blunted Cone, 5-segment SRM's
22	Titan III-C, Centaur/Voyager with small and large forward vortex generators, 5-segment SRM's
24	Titan III-C, Centaur/Voyager, 7-segment SRM's
25	Titan III-C, Centaur/Voyager with Shroud C and small forward vortex generators, 5-segment SRM's
26	Titan III-C, Centaur/Voyager with small forward vortex generators, 5-segment SRM's
27	Titan III-C, Transtage, Centaur/Gemini, 5-segment SRM's

PHASE III TEST CONFIGURATIONS

Configuration Number	Configuration Description
30	Titan III Stretched Core, Transtage/Std 21,000-lb fairing, 7.5-segment SRM's
31	Titan III Stretched Core, MOL with Protuberances/Gemini, 7.5-segment SRM's
32	Titan III Stretched Core, MOL/Conical Nose, 7.5-segment SRM's
33, 41*	Titan III Stretched Core, MOL/Gemini, 7.5-segment SRM's
34	Titan III Stretched Core, MOL/SV-5, 7.5-segment SRM's
35	Titan III Stretched Core, 13-ft-diam, 20-ft-long Cylinder/Apollo without launch escape tower, 7.5-segment SRM's
36	Titan III Stretched Core, 13-ft-diam, 20-ft-long Cylinder/Apollo with long launch escape tower, 7.5-segment SRM's
37	Titan III Stretched Core, 13-ft-diam, 40-ft-long Cylinder/Apollo with long launch escape tower, 7.5-segment SRM's
40	Titan III Stretched Core, 13-ft-diam, 20-ft-long Cylinder/Apollo with short launch escape tower, 7.5-segment SRM's

*Configurations 33 and 41 were geometrically the same; the difference was that configuration 41 had lower structural damping.

SECTION I
INTRODUCTION

As launch vehicles pass through the transonic Mach number range, they are subjected to large unsteady aerodynamic forces. These forces may generally be categorized as (1) buffet loads which produce elastic deformations of the entire vehicle, and (2) buffet loads which affect local panels and vehicle components composing the external surface of the vehicle. In both cases, important aeroelastic problems arise which, because of the lack of theoretical methods to predict the buffet loads, may be solved only through experimental investigation. There are two basic experimental techniques employed to analyze the response of the vehicle to buffet loads. The first involves direct measurement of the unsteady aerodynamic forces by distributing a large number of unsteady pressure sensors over the vehicle surface. Correlation techniques are applied to the measured unsteady pressures to form a matrix of the forcing function. By properly defining the transfer function based on the elastic characteristics of the missile structure, the vehicle response may be determined analytically from the matrix of the forcing function. The second, more direct, method of measuring the vehicle response to buffet loads involves fabricating an aeroelastic model which is dynamically similar to the prototype vehicle. The response is measured directly by bending-moment sensors attached to the model structure. By properly employing the scaling relationships, the model results may be adjusted to full scale, and reasonable estimates of the prototype-vehicle response are obtained. Because of the small scale of most wind tunnel models it is not feasible to aeroelastically scale the panels and components composing the external surface of the vehicle. Thus, the unsteady pressure sensor approach is usually employed to analyze the response of these structures to local buffet forces.

The primary objective of the present investigation was to measure, for various payload and booster configurations, the structural response of 0.07-scaled, aeroelastic models of Titan III missile configurations to buffet airloads at transonic Mach numbers. A secondary object was to obtain sound-pressure levels at various locations on the model surface to assist in defining the effects of local buffet forces. The tests were conducted in the Propulsion Wind Tunnel, Transonic (16T) at AEDC during the periods from January 18 through 27, 1966, March 14 through 16, 1966, May 2 through 18, 1966, and October 31 through November 10, 1966. The first three test periods constituted the Phase II Wind Tunnel Test Plan, and the last entry was the first of a series of entries categorized as the Phase III Wind Tunnel Test Plan.

SECTION II
APPARATUS

2.1 TEST FACILITY

Tunnel 16T is a variable density wind tunnel. The test section is 16 ft square and is lined with perforated plates to allow continuous operation through the Mach number range from 0.55 to 1.60 with minimum wall interference.

Details of the test section showing the locations of the models and support strut arrangements are presented in Figs. 1 and 2 (Appendix I) for the Phase II test configurations and in Fig. 3 for the Phase III test configurations. A more extensive description of the tunnel is given in Ref. 1, and the latest calibration results are presented in Ref. 2.

2.2 TEST ARTICLES

The test articles were aeroelastically scaled Titan III missile configurations. The model physical properties are presented in Appendix II, and details of the model scale factors are presented in Appendix III. The configurations consisted of single-body (Titan III-A) and three-body (Titan III-C) boosters with various upper stages and payloads. A summary of the various configurations tested during the Phase II and Phase III entries and corresponding configuration numbers are presented in the nomenclature.

2.2.1 Phase II Test Configurations

The booster for the single-body, Titan III-A configuration consisted of a 120-in.-diam Titan III core as shown in Fig. 4a. The booster for the three-body, Titan III-C configurations consisted of the 120-in.-diam Titan III core centerbody and two 121-in.-diam strap-on, solid-rocket motors (SRM). The strap-on rockets were either the standard 5-segment SRM's or the longer 7-segment SRM's. Details of the Titan III-C boosters are presented in Fig. 4b. The upper stage (stage III) of each configuration was either the Martin Transtage (Fig. 4a) and/or the General Dynamics/Astronautics Centaur stage (Fig. 4b).

The payloads were as follow:

1. Standard fairings (10-ft-diam cone-cylinder payload), configurations 1 and 2, Fig. 5a.

2. The 15-ft-diam bulbous payload, configuration 9, Fig. 5a.

3. Voyager with four different shrouds (18-ft-diam bulbous payloads), configurations 3 through 6, Fig. 5b.

4. The 13-ft-diam Manned Orbiting Laboratory (MOL) payloads (20- and 40-ft-long cylinders), configurations 19 and 20, Fig. 5c.

5. The 10-ft-diam MOL/Gemini payload (the Martin transtage and the GD/A Centaur were stacked to simulate a 10-ft-diam MOL cylinder), configuration 27, Fig. 5c.

The basic Centaur/Voyager (configuration 3) and the Centaur/Voyager with shroud C (configuration 6) were also tested with modifications to the payloads. These modifications are illustrated in Fig. 6.

2.2.2 Phase III Test Configurations

The boosters for all Phase III test configurations were three-body configurations consisting of a modified Titan III core centerbody and two 121-in.-diam, 7.5-segment SRM's. (The core used for the Phase II test was extended in length to accommodate the 7.5-segment SRM's). The modified core is referred to as the Titan III stretched core. Details of the Phase III booster are presented in Fig. 7.

Basic payloads were as follow:

1. Standard fairing (same as configuration 2 payload), configuration 30, Fig. 8a.

2. The 10-ft-diam MOL with three different payloads, configurations 32, 33, and 34, Fig. 8a.

3. The 13-ft-diam Apollo with different escape tower and cylinder lengths, configurations 35, 36, 37, and 40, Fig. 8b.

In general, the reaction control rockets were the only protuberances external to the MOL cylinder (Fig. 9). However, one MOL configuration was tested with four additional protuberances (configuration 31) as illustrated in Fig. 9.

2.2.3 Model Construction

Some of the details of the model construction are shown in photographs of the model at various stages of the assembly in Fig. 10. The model consisted of the following components:

1. Sting support system, Fig. 10a.
2. Elastic structure with concentrated weights, Fig. 10b.
3. External skin, Fig. 10c.

The model sting support system for the three-body configurations consisted of three steel pipes cantilevered from a cross member which attached to the PWT sting system. The long center prong entered the model core and the shorter outside prongs entered the SRM's. For the single-body configuration (configuration 1), the two outside prongs and the cross member were removed, leaving only the core prong.

The models were supported on the sting by spring systems housed inside the sting. The spring support system was designed to restrain the model in the axial direction, support the model weight, and to provide a minimum of restraint to motion in the pitch and yaw free-free bending modes. Schematics of the spring support systems for the single- and three-body configurations are shown in Figs. 11 and 12, respectively. For the single-body configuration, the model structure was supported at two points – near the forward and rear nodes of the first pitch and yaw free-free bending modes. For the three-body configurations, the model structure was supported at three points – at the upstream end of the core and at the downstream end of each SRM. These points also corresponded closely to the nodes of the first pitch and yaw free-free bending modes. As the model weight was changed or as the model was pitched to angle of attack, the change in load on the support springs caused the model to be vertically displaced off the centerline of the sting. The model was re-centered by pitching the cantilevered end of the springs. This was accomplished by remote-controlled, electric-powered pitch systems housed inside the sting. In addition to the spring support system, the model sting housed a snubber and brake system to lock the model when excessive rigid body vibrations were encountered. A fouling system was connected to the snubber to indicate interference in the rigid body modes. A second brake system was located in the payloads to lock the model when excessive vibrations in the elastic modes were encountered. The payload brake was attached to a spike which in turn was connected to the core prong. An analysis of the effects of the spring support system on the bending-moment response of the model is presented in Section 4.4

The structural backbone of the model was the core, stage III, and SRM elastic structures. The core and stage III structures were constructed of 2024-T4 aluminum tubing, and the SRM structures were constructed of 6061-T6 aluminum tubing. The tubes were machined to satisfy the scale stiffness requirements. Steel weights were attached to the elastic structures to simulate the running inertia and mass characteristics.

The correct aerodynamic form was obtained by covering the skeleton structures with aluminum and/or balsa wood cylindrical segments. The joints between the aluminum segments were sealed with a silastic rubber which enabled the segments to move independently and thus not restrain the model in bending.

The payloads were constructed of a skeleton of aluminum and plywood with the external contour shaped from balsa wood and fiber glass. The payload weight, center of gravity, and mass moment of inertia were simulated; however, except for the Phase III MOL section, the stiffness was higher than that dictated by similitude laws. The MOL section was constructed of 7075-T6 aluminum tubing and chemically milled to obtain the correct scaled stiffness distribution. Balsa wood was bonded directly to the MOL aluminum structure to obtain the correct aerodynamic geometry.

2.3 INSTRUMENTATION

2.3.1 Model

Instrumentation in the model consisted of the following:

1. Pitch and yaw bending-moment sensors located on the core and Phase III MOL structures.
2. Normal- and side-force sensors located on the support springs.
3. Pitch and yaw accelerometers located in the model payloads.
4. Position sensor located at the forward support spring attachment point.
5. Microphones distributed on the model surface.

The bending-moment and force sensors were strain-gage bridges with four active arms. The gages of the bending-moment sensors were bonded to the exterior of the core and MOL structures such that the geometric center of the sensors was at the model centerline. The gages of the force sensors were bonded to the support springs, and the geometric centers of the sensors were at the spring centerlines. Typical core and spring cross sections showing details of the gage installations are presented in Fig. 13. Axial locations of the bending-moment sensors are presented in Fig. 14a for the Phase II test configurations and in Fig. 14b for the Phase III test configurations.

Two crystal accelerometers were installed in the payloads. One accelerometer was sensitive to motion in the pitch plane, and the other

was sensitive to motion in the yaw plane. The axial location of the accelerometers varied with payload configuration changes.

The position sensor located at the forward support spring attachment point measured the vertical displacement of the model from the center of the sting support. This sensor was a linear potentiometer for the Phase II test configurations and a differential transformer for the Phase III test configurations. The differential transformer proved to be the more reliable position sensor.

Up to ten microphones were distributed over the model to measure local sound-pressure levels. The microphones were of secondary importance to the test, and since the microphone results are omitted from this report, their locations are not presented.

2.3.2 Data Recording and Monitoring

Outputs from the model instrumentation were conditioned and recorded and/or monitored on-line as illustrated in Fig. 15. Dynamic measurements were recorded on two magnetic-tape systems and two oscillographs. Up to four root-mean-square (rms) voltmeters were used to obtain on-line readings during the test. Steady-state measurements were processed through the PWT force and moment readout system described in Ref. 1. Also, a schlieren system was used to obtain still and motion pictures of the flow about the models.

Oscilloscopes and television cameras, in addition to the data recording instrumentation, were used to monitor the model during the test.

SECTION III
TEST DESCRIPTION

3.1 TEST CONDITIONS

The tests were conducted in the Mach number range from 0.60 to 1.40 and at angles of attack ranging from 0 to 4 deg. Tunnel stagnation temperature ranged from 100 to 110°F. To satisfy model scaling parameters (see Appendix III), it was necessary to test at dynamic pressures corresponding to the full-scale flight trajectories. Variations of the dynamic pressure (q_∞) with Mach number (M_∞) for the various configurations are presented in Fig. 16. The dynamic pressure variations in Fig. 16 represent the upper limit of the q_∞ dispersions for the full-scale flight trajectories and are referred to as the normal q_∞ schedules.

The resulting variations in Reynolds number, based on the model core diameter, are presented in Fig. 17. It should be pointed out that the necessity to match dynamic pressure resulted in a mismatch in Reynolds number between the model and the prototype vehicle. This mismatch was not considered detrimental to the purpose of the test (see Ref. 3).

In addition to the tests conducted at the normal q_∞ schedules (Fig. 16), the effects of variations in dynamic pressure were investigated for the Mach number range of peak buffet response. These dynamic pressures (q'_∞) ranged within ±20 percent of the normal q_∞ schedules.

3.2 TEST PROCEDURE

The test consisted of two distinct phases (1) model vibration testing before air-on testing and (2) air-on buffet testing.

3.2.1 Model Vibration Tests

The model vibration tests were conducted to establish the model rigid body and elastic modal characteristics (in both pitch and yaw) when supported by the model sting system and the remaining PWT sting assembly. These tests were conducted on each configuration in the tunnel before the air-on tests and in the following manner:

1. An electromagnetic shaker driven by a variable frequency oscillator was connected to the payload of each configuration, and a reference accelerometer was attached to the model at a station near the payload.
2. Each of the first two rigid body modes (translation and rotation) and the first three elastic modes in both pitch and yaw were excited by the shaker and "tuned" by monitoring Lissajous displays of the shaker input and accelerometer output on an x-y oscilloscope.
3. After each mode was properly tuned, the modal response frequencies were recorded. A second roving accelerometer was attached to the model near the fixed accelerometer, and the roving and fixed accelerometer outputs were connected to the x and y axes of an oscilloscope, respectively. The desired modal frequency was tuned, and the phase angle of the two accelerometer outputs as displayed on an oscilloscope was adjusted to unity. The modal shape was determined by moving the roving accelerometer to various predetermined stations

along the length of the model and recording the phase angle from the oscilloscope displays. This procedure was repeated for each mode.

4. After each modal shape survey, the outputs of the bending-moment sensors for each modal frequency were recorded on magnetic tape and on an oscillograph. The oscillograph data provided a quick check of the bending-moment sensors and the bending-moment sensitivity distribution of the configuration.

5. The damping of each elastic mode was determined by exciting the modes, removing the excitation force instantaneously, and recording the resulting decays on an oscillograph. This procedure was repeated at various amplitudes of excitation to determine the effect of amplitude on the damping characteristics of each mode.

3.2.2 Air-On Buffet Testing

Because of the nature of the test, it was necessary to proceed to desired test conditions with extreme caution. Before tunnel start, the model was locked, utilizing the rigid body and elastic vibration brake systems discussed in Section 2.2.3. After the flow was established at a low dynamic pressure, the model was unlocked. Dynamic pressure was increased until the desired test conditions were realized and the data were recorded. All bending-moment and force sensors were monitored to ensure that loads in excess of the structural capability of the model were not reached. In the event that excessive loads were encountered (flutter for example, as was the case for several configurations), the model was immediately locked utilizing first the rigid body brake systems and second the elastic vibration brake system.

3.3 DATA REDUCTION

Steady-state force and bending-moment measurements and test conditions were reduced and tabulated on-line. The steady-state force and moment results were used primarily to monitor the test and are not presented herein.

The buffet response bending-moment, accelerometer, and microphone measurements as recorded on magnetic tape will be reduced by the Martin-Marietta Corporation, Denver Division. Selective rms bending-moment measurements were hand recorded during the test. The bending-moment sensors selected were the pitch and yaw sensors

most sensitive in the first elastic pitch and yaw bending modes, respectively. These data were obtained using time-integrated, rms voltmeter systems developed in PWT. The real time data sample for the rms analysis was 50 sec. Also, the selected bending-moment sensor outputs were filtered to exclude the rigid body frequencies and thus obtain the bending moments resulting from vibration in the elastic modes. The on-line bending-moment results are presented herein.

3.4 PRECISION OF MEASUREMENTS

The uncertainties in setting and maintaining test conditions are estimated to be as follow:

Mach number	±0.005
Dynamic pressure	±4 psf
Angle of attack	±0.10 deg

The Mach number uncertainty does not include the longitudinal variation in the tunnel test section. Maximum variations from the average Mach number in the vicinity of the test articles ranged from ±0.005 at subsonic Mach numbers to ±0.015 at supersonic Mach numbers (Ref. 2).

The uncertainties in the fluctuating bending moments based on the pre- and post-test calibrations of the bending-moment sensors are estimated to be as follow:

$$\text{Phase II} \begin{cases} \text{Pitch } \Delta\sigma_M = \pm 0.010\ \sigma_M \\ \text{Yaw } \Delta\sigma_M = \pm 0.005\ \sigma_M \end{cases}$$

$$\text{Phase III} \begin{cases} \text{Pitch } \Delta\sigma_M = \pm 0.002\ \sigma_M \\ \text{Yaw } \Delta\sigma_M = \pm 0.004\ \sigma_M \end{cases}$$

The bending-moment uncertainties do not include statistical errors resulting from nonstationarity of the measurements.

SECTION IV
RESULTS AND DISCUSSION

4.1 GENERAL

Variations of the total elastic rms bending moment (σ_M) resulting from buffet airloads with free-stream Mach number (M_∞) are presented

in Figs. 18 and 19 for the Phase II and III test configurations, respectively. These results were obtained by hand recording rms voltages of the selected bending-moment sensor outputs during the test. The bending-moment sensors with stations as noted in Figs. 18 and 19 were selected because of their close proximity to the station of peak bending-moment sensitivity for the first pitch and yaw elastic bending modes, as mentioned in Section 3.3. For some configurations, it was necessary to use a less sensitive sensor because of failure of the primary sensor. Thus, a comparison of the bending moments between configurations should not be made. Also, it should be noted that the bending-moment sensor outputs were filtered below 10 cps to exclude the rigid body frequencies of the support springs from the rms measurements. A discussion of the effects of the support springs on the structural response of the models is presented in Section 4.4.

4.1.1 Phase II Test Results

Variations of σ_M with M_∞ for the single-body, Titan III-A configuration (configuration 1, Fig. 18a) indicate a relatively low structural response, especially in pitch, and are probably indicative of model response to the tunnel free-stream disturbances. Also, configuration 1 exhibited little variation of σ_M with M_∞, whereas the three-body, Titan III-C configuration with the same geometry payload (configuration 2, Fig. 18b) experienced peak response in the Mach number range from 0.80 to 0.90.

The primary configurations for the Phase II test were the Centaur/Voyager configurations. The basic Centaur/Voyager (configuration 3) experienced flutter in the first pitch and yaw bending modes as Mach number was increased above 0.80 (Fig. 18d). The flutter was alleviated by adding to the payload a cylindrical shroud of the same diameter as the payload (shroud B, configuration 5, Fig. 18i). The Centaur/Voyager with a shroud of smaller diameter than the payload (shroud A, configuration 4) also experienced flutter. Tests of this configuration at Mach numbers above 1.0 indicated that the flutter Mach number regime was from approximately 0.80 to 1.00, as shown in Fig. 18h. The Centaur/Voyager with a boattail shroud (shroud C, configuration 6) experienced flutter near $M_\infty = 0.90$; however, the flutter was eliminated by adding a ring of vortex generators to the payload immediately upstream of the shroud (configuration 25) as shown in Fig. 18j. The addition of vortex generators and splitter plates to the basic Centaur/Voyager (configurations 15, 16, 17, 22, and 26) was unsuccessful in eliminating the flutter instability, as shown in Fig. 18.

4.1.2 Phase III Test Results

Variations of σ_M with M_∞ for the standard cone fairing configuration (configuration 30), Fig. 19a, were similar to those for configuration 2 which had a shorter booster. The Mach number range of peak structural response was from 0.80 to 0.90.

The MOL family of configurations consisted of several payload geometries; however, variations of σ_M with M_∞ for all configurations were similar (Figs. 19b through f). Bending moments were relatively large in the range $0.8 \leq M_\infty \leq 1.0$, and a small, sharp peak occurred at $M_\infty = 0.95$. In general, variations of σ_M with M_∞ for yaw were less than the variations for pitch.

Variations of σ_M with M_∞ for the Apollo configurations were somewhat different in appearance from the MOL variations, as shown in Figs. 19g through j. The maximum structural response for the Apollo configurations occurred in the Mach number range from 0.90 to 0.95.

4.2 EFFECTS OF DYNAMIC PRESSURE

The effects of variations in dynamic pressure about the normal q_∞ schedule were investigated for the Phase III MOL and Apollo configurations, and the results are presented in Figs. 20 and 21, respectively. In Figs. 20 and 21, the rms bending moments at off-normal dynamic pressures are plotted versus the rms bending moments at normal dynamic pressure where each point represents a given Mach number. The data were obtained for the Mach number range of peak buffet response (from 0.80 to 1.20). Although there is considerable scatter in the results, it is evident that the structural response in both pitch and yaw varied with dynamic pressure. The rms bending moments for dynamic pressures 20 percent below the normal q_∞ (σ'_M) were less than those recorded at normal q_∞ (σ_M) in both pitch and yaw as shown in Fig. 20 for the MOL configuration and in Fig. 21 for the Apollo configuration. Similarly, a 20-percent increase in dynamic pressure caused the structural response to increase as shown in Fig. 21 for the Apollo configurations.

From an analysis of the structural response presented in Ref. 4, it was shown that, for the case where aerodynamic damping is large relative to structural damping, the rms bending moment varies with the square root of the dynamic pressure. That is, for the case where

$$C_A \gg C_s + C_c$$

then

$$\sigma_M \propto \sqrt{q_\infty}$$

For the case where aerodynamic damping is small relative to structural damping

$$C_A \ll C_s + C_c$$

then

$$\sigma_M \propto q_\infty$$

The results presented in Figs. 20 and 21, in general, indicate that the rms bending moments varied as the first power of the dynamic pressure and therefore suggest that the aerodynamic damping was relatively small. The structural damping was generally less than 3 percent of critical damping for the present configurations (see Appendix II). For the prototype vehicles, the structural plus control-systems damping is estimated to range from 3.5 to 4.5 percent of critical damping for the first elastic mode. Damping in the higher modes is estimated to be one percent of critical damping.

4.3 EFFECTS OF ANGLE OF ATTACK

The effects of angle of attack were investigated for certain Phase II and III test configurations, and the results are presented as variations of σ_M with α for both pitch and yaw. The results for the Phase II and III test configurations are shown in Figs. 22 and 23, respectively. The angles of attack for each configuration depended on the loads experienced versus the stress capability of the model and ranged from 0 to 4 deg.

The buffet loads experienced by the single-body, Titan III-A (configuration 1) were essentially invariant with angle of attack as shown in Fig. 22a. Increasing the angle of attack resulted in a noticeable decrease in the pitch bending-moment response for the three-body, Phase II test configurations (Figs. 22b through f). One exception was configuration 19 at $M_\infty = 1.0$ (Fig. 22e), and this trend may have been affected by nonstationarity of the structural response (see Section 4.4). In general only slight variations with angle of attack were observed in yaw structural response for the Phase II test configurations.

The effects of angle of attack on the structural response of the Phase III test configurations other than configurations 30 and 32 are inconclusive because of the restricted range of angles of attack investigated and the nonstationarity of the results. The structural response for configuration 30 increased in pitch and yaw at 1-deg angle of attack and decreased as angle of attack was increased above 1 deg (Fig. 23a).

Configuration 32 experienced a decrease in structural response in pitch and yaw with increasing angle of attack (Fig. 23c).

4.4 EFFECTS OF SPRING SUPPORT SYSTEM

The bending moments presented in Figs. 18 through 23 are indicative of structural response of the model in the elastic bending modes since the response in the lower frequency domain was filtered. However, it is interesting to note the effect of the spring support system as indicated by comparing the total unfiltered bending moments (σ_{M_T}) with the total elastic bending moments (σ_M). The results are presented quantitatively for representative configurations in Figs. 24a and b for pitch and yaw, respectively. The support springs increase the rms bending moments approximately 25 percent in pitch (Fig. 24a), whereas their effect was negligible in yaw (Fig. 24b). The scatter in the results presented in Fig. 24 indicates that the structural response was nonstationary. Values of σ_{M_T} were recorded approximately 2 min after the recording of σ_M. Nonstationarity was also observed from successive readings of σ_M, as shown for a few conditions in Fig. 18.

4.5 FLOW VISUALIZATION

Schlieren photographs of the flow about the model payloads were obtained for most configurations in the Mach number range from 0.60 to 1.40. Typical examples are presented in Figs. 25a and b for a MOL configuration (configuration 31) and an Apollo configuration (configuration 37), respectively. The schlieren photographs show large regions of separated flow surrounding the payloads, and for $M_\infty \geq 0.90$, the formation of shock waves on the MOL and Apollo cylinders.

4.6 APPLICATION OF RESULTS

The designer is obviously concerned with more than the bending moment at a single vehicle station as presented herein. To properly analyze the total vehicle structure, the distribution of the buffet bending moments along the vehicle is required. In order to obtain the full-scale bending-moment distribution it is necessary to (1) determine the bending-moment sensitivity along the model for each elastic mode, (2) determine the modal contributions to the total elastic bending moments resulting from buffet airloads as measured from a wind tunnel model, (3) determine the full-scale modal contributions by proper application of scaling relationships, (4) determine the full-scale

bending-moment distributions for each mode, and (5) determine the resultant bending-moment distribution by summing the distributions of each mode. The vehicle is usually designed to some appropriate safety factor. The present vehicle will be designed to a factor of 3 σ_M (full scale).

Analysis of the test results to obtain the full-scale bending-moment distributions will be conducted by Martin-Marietta Corporation, Denver Division, and because of the time involved, these results were not included in this report.

SECTION V
CONCLUSIONS

On the basis of wind tunnel tests conducted on aeroelastically scaled Titan III missile configurations, the following conclusions can be drawn:

1. The single-body, Titan III-A configuration experienced relatively low buffet loads and exhibited little variation of buffet bending moments with Mach number.
2. The three-body, Titan III-C configurations with a standard cone payload fairing experienced peak response to buffet loads in the Mach number range from 0.80 to 0.90.
3. The basic Centaur/Voyager configuration experienced a flutter instability in the first elastic pitch and yaw bending modes as Mach number was increased above 0.80. This instability was eliminated by (a) adding to the payload a cylindrical shroud having the same diameter as the payload and (b) adding to the payload a boattail shroud with a ring of vortex generators upstream of the boattail.
4. The MOL configurations investigated during the Phase III test experienced peak structural response to buffet airloads at Mach numbers near 0.95.
5. The Apollo configurations investigated during the Phase III test experienced peak bending-moment response to buffet airloads at Mach numbers near 0.95; however, the trends with Mach number were somewhat different from the trends for the MOL configurations.
6. Increasing dynamic pressure caused a proportionate increase in the pitch and yaw structural response.

7. Variations of rms bending moment with angle of attack, in general, indicated that the structural response in pitch and yaw decreased with increasing angle of attack. However, there were deviations from this trend for certain configurations.

REFERENCES

1. Test Facilities Handbook (6th Edition). "Propulsion Wind Tunnel Facility, Vol. 5." Arnold Engineering Development Center, November 1966.

2. Chevalier, H. L. "Calibration of the 16-foot Transonic Circuit with a Modified Model Support System and Test Section." AEDC-TN-60-164 (AD241785), August 1960.

3. Pretest Report on 7% Transonic Buffet for Various Titan III Configurations. Martin-Marietta Corporation, Denver Division, Martin-Denver SSD-CR-65-257, January 1966.

4. Doggett, Robert V., Jr. and Hanson, Perry W. "An Aeroelastic Model Approach for the Prediction of Buffet Bending Loads on Launch Vehicles." NASA TN D-2022, October 1963.

APPENDIXES

I. ILLUSTRATIONS
II. TABLES
III. MODEL SCALING

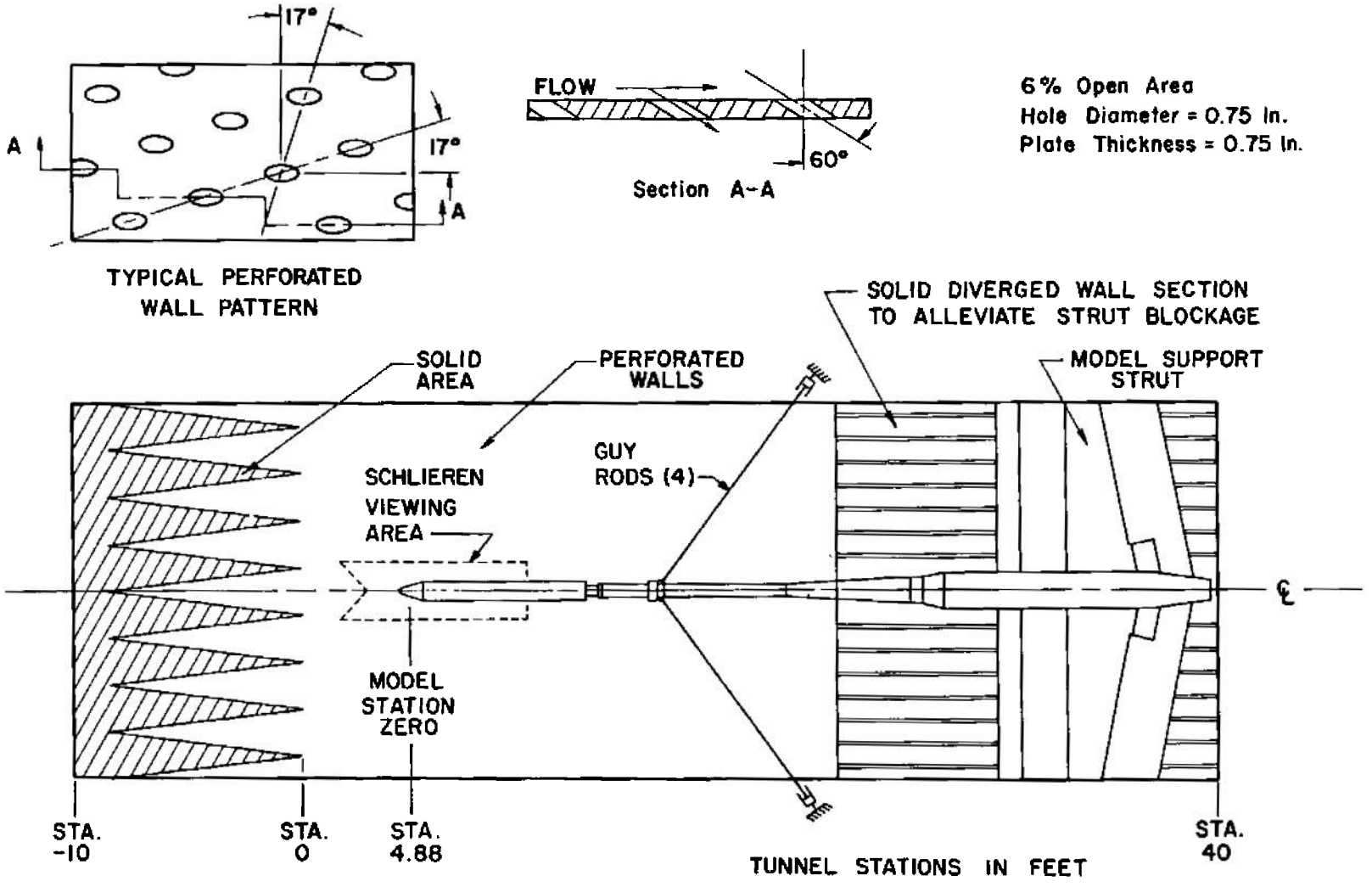

a. Installation Schematic

Fig. 1 Details of the Single-Body, Titan III-A Model Installation in the Tunnel

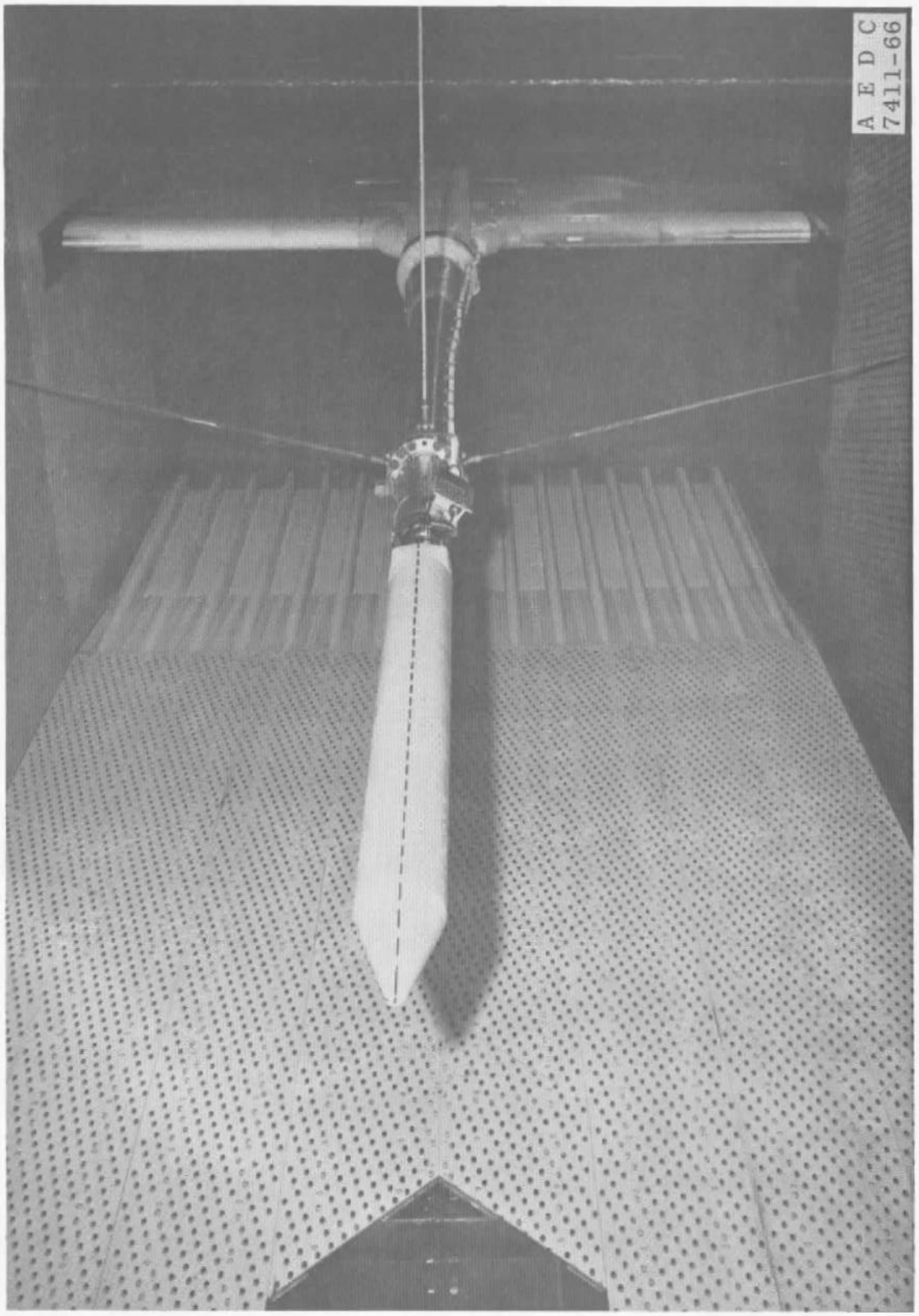

b. Installation Photograph

Fig. 1 Concluded

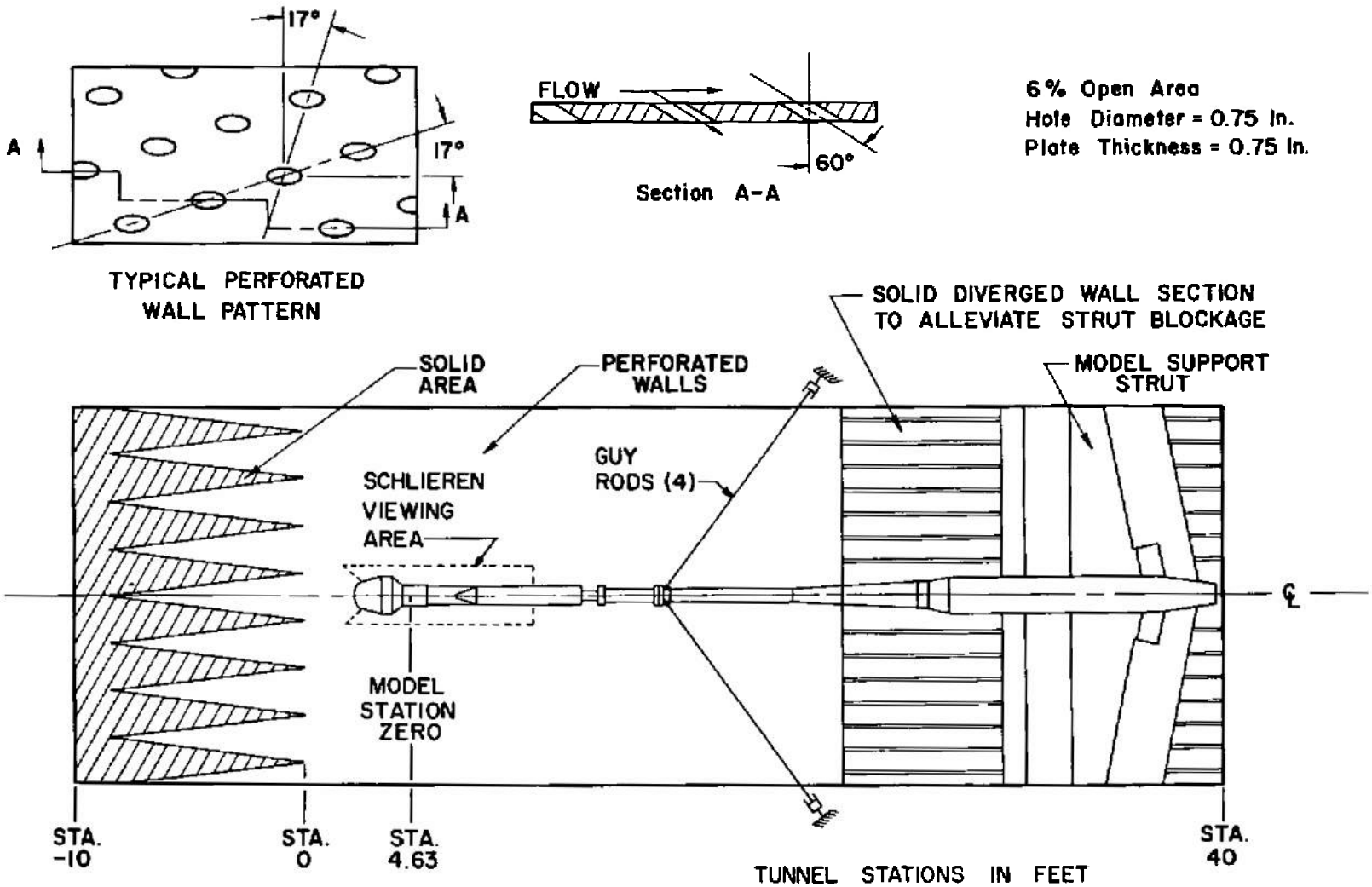

a. Installation Schematic

Fig. 2 Details of a Typical Three-Body, Titan III-C Model Installation in the Tunnel, Phase II Test

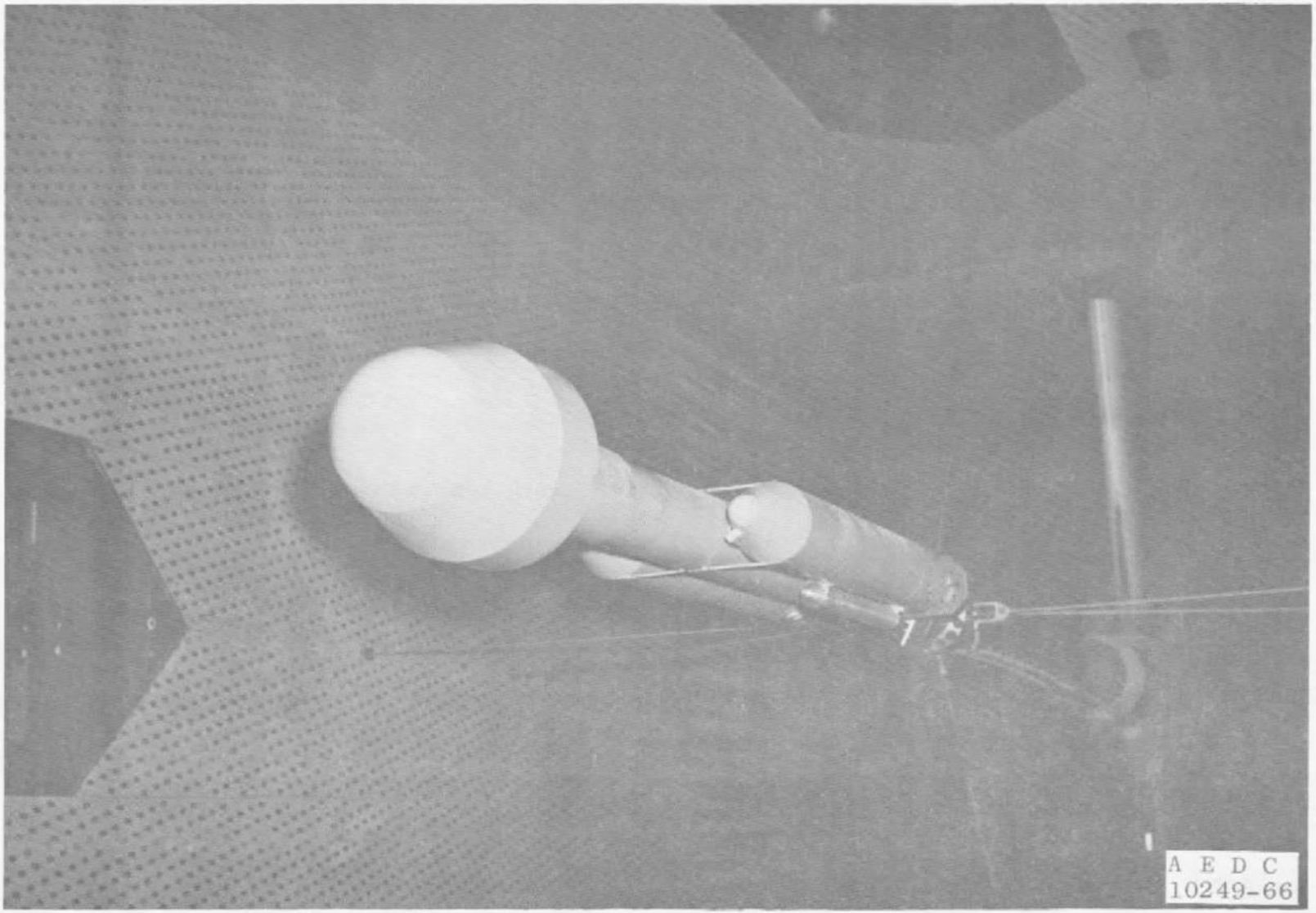

b. Installation Photograph

Fig. 2 Concluded

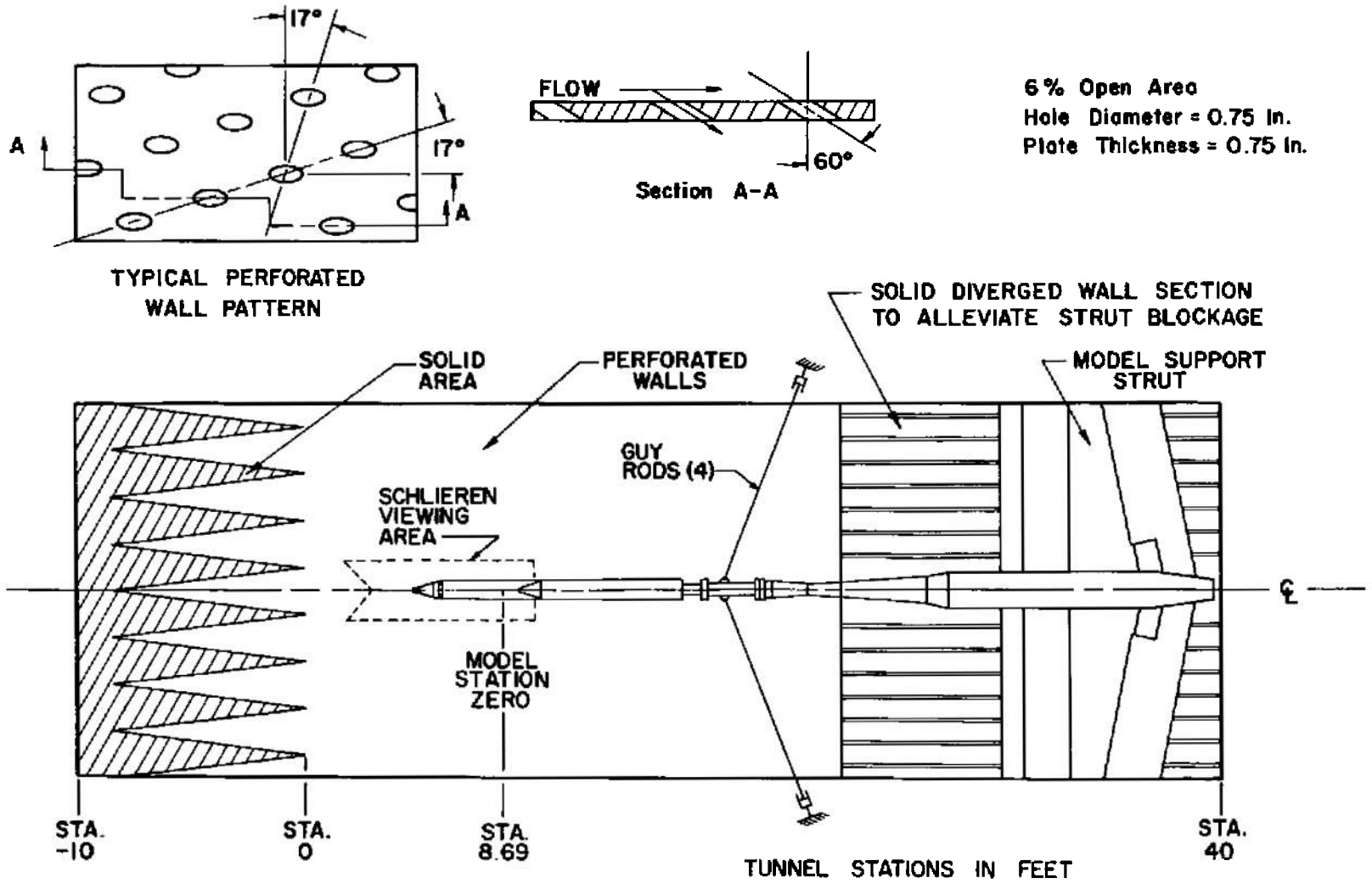

a. Installation Schematic

Fig. 3 Details of a Typical Three-Body, Titan III Model Installation in the Tunnel, Phase III Test

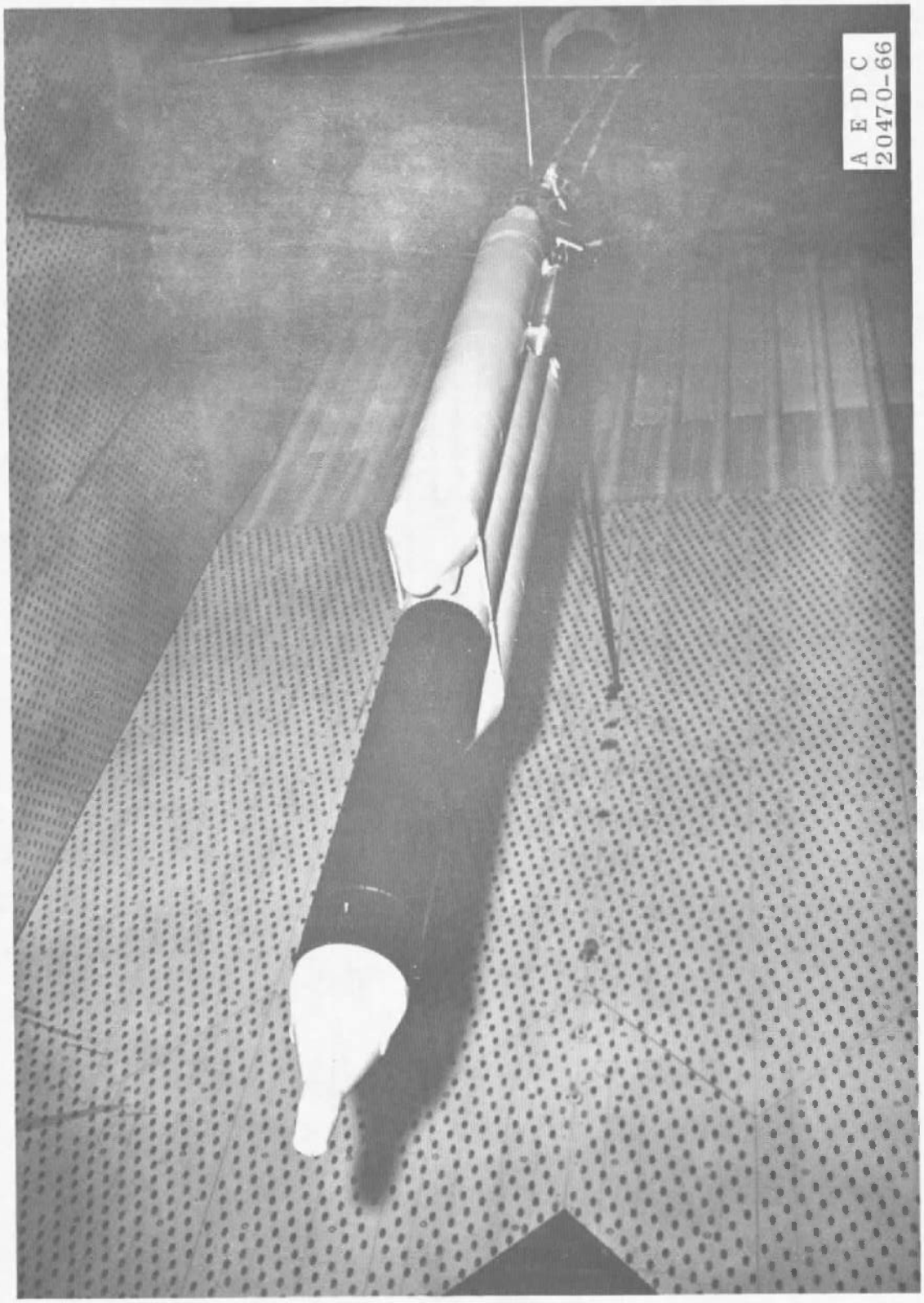

b. Installation Photograph

Fig. 3 Concluded

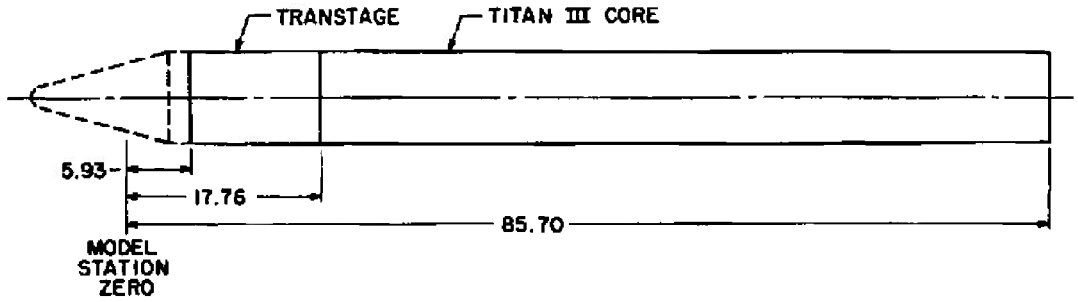

a. Single-Body, Titan III-A Configuration

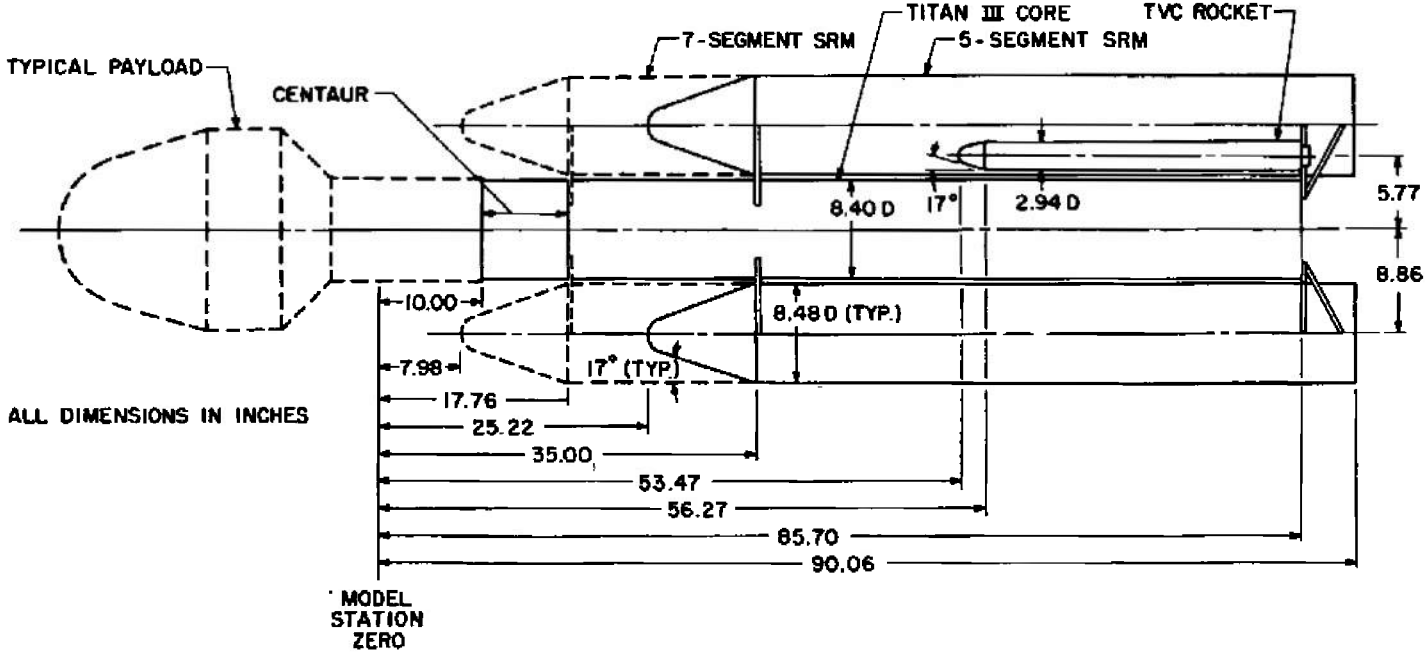

b. Three-Body, Titan III-C Configurations

Fig. 4 Details of the Boosters for the Phase II Test Configurations

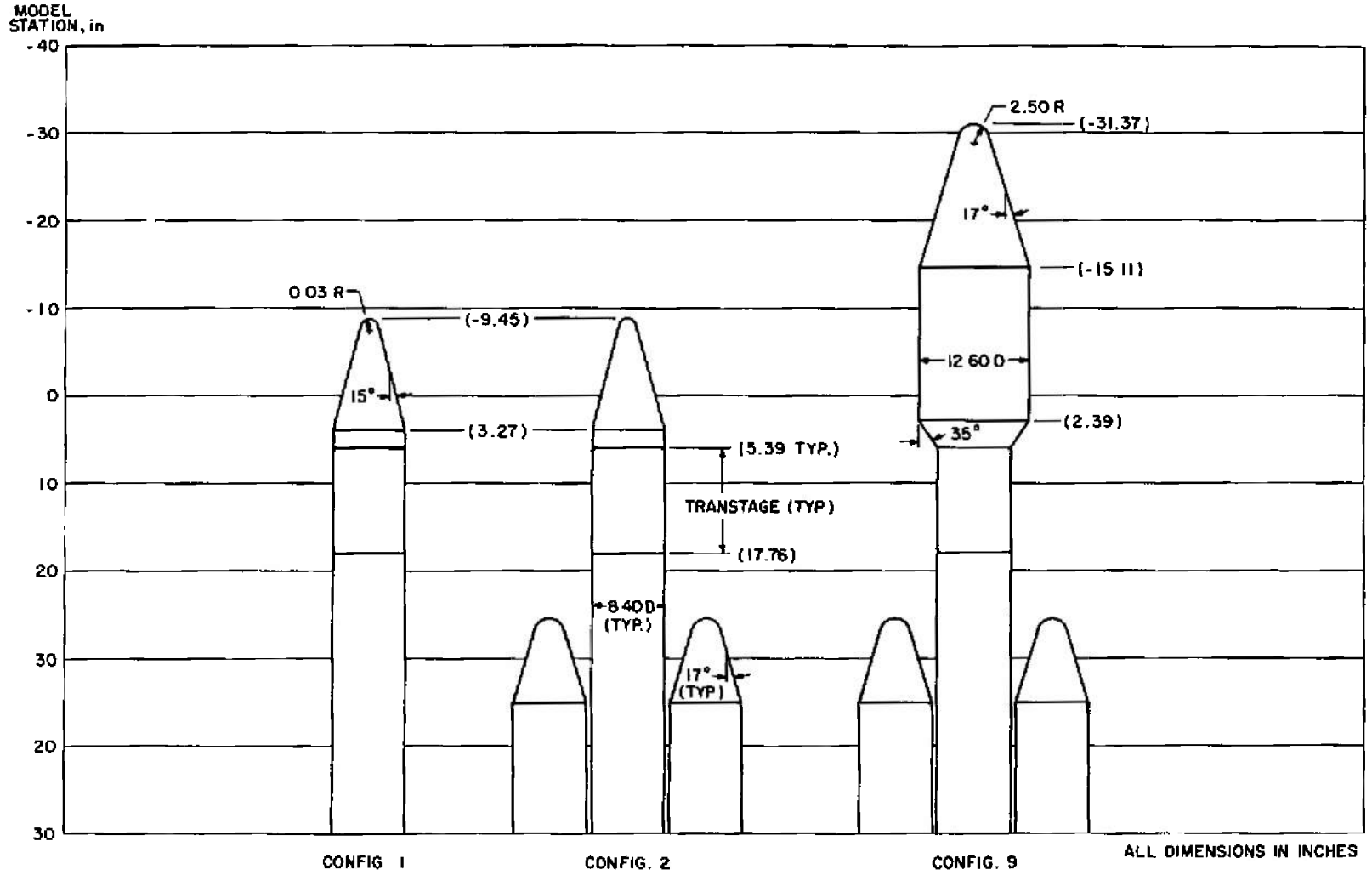

a. Configurations 1, 2, and 9

Fig. 5 Details of the Payloads for the Phase II Test Configurations

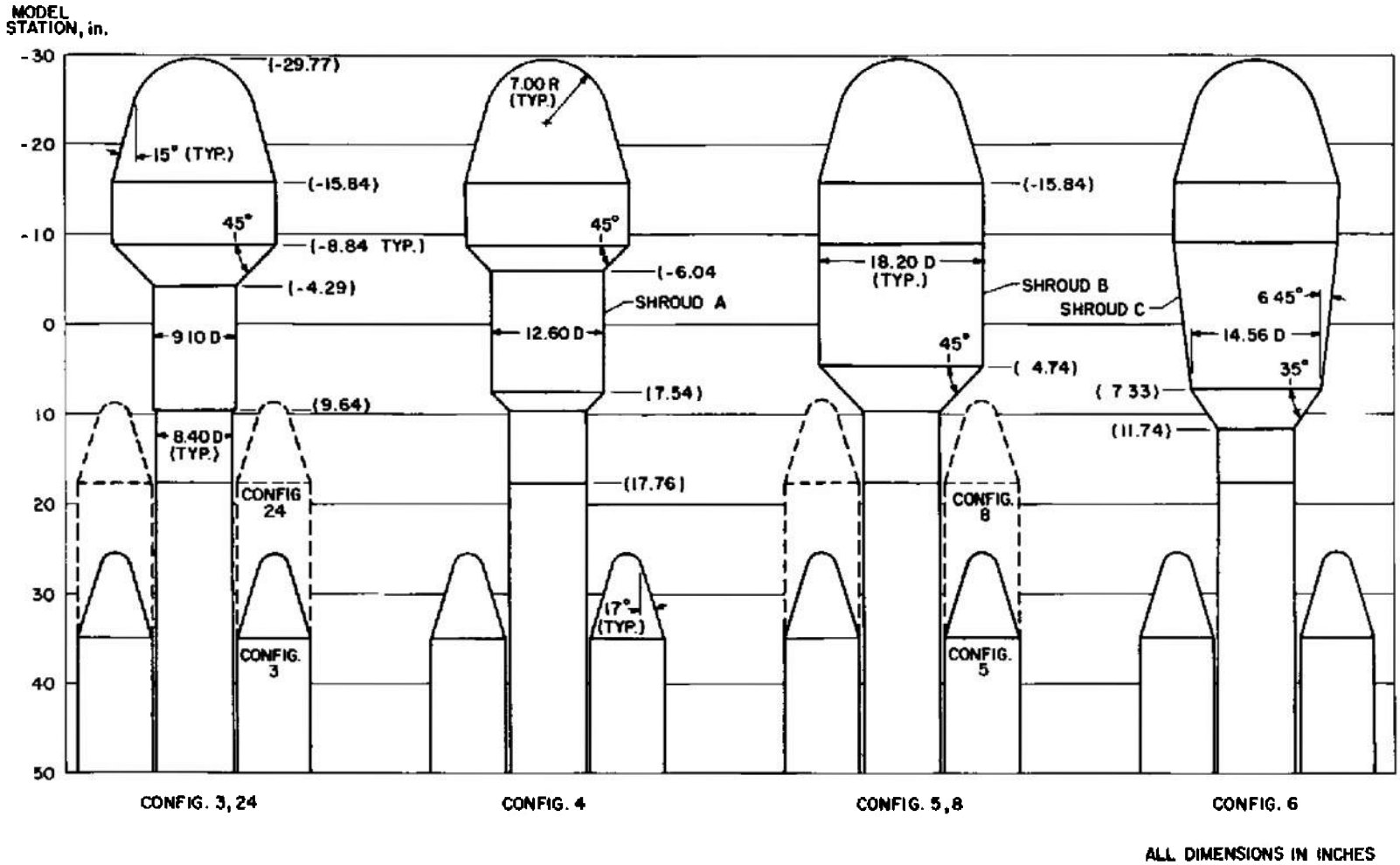

b. Configurations 3, 4, 5, 6, 8, and 24

Fig. 5 Continued

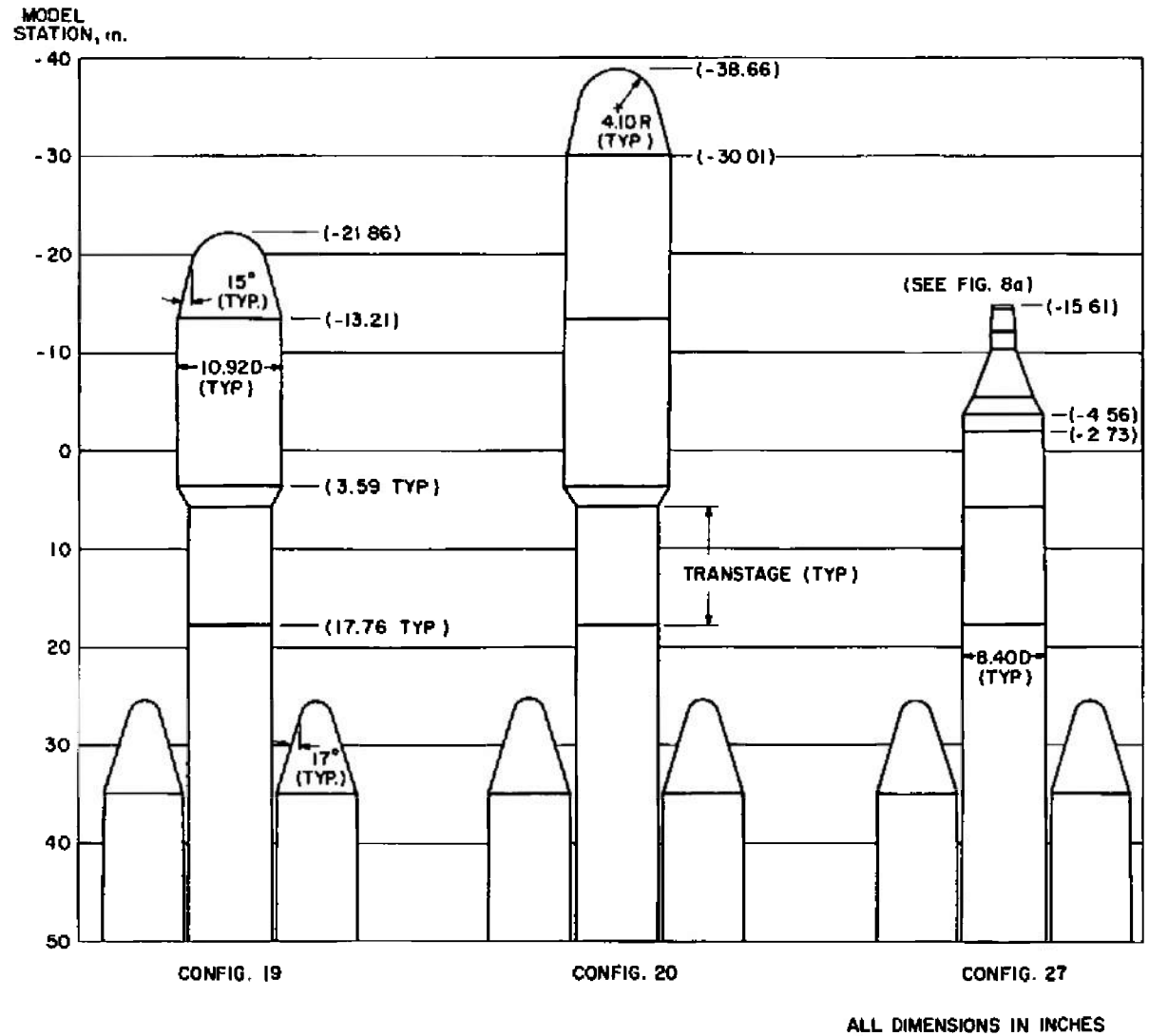

c. Configurations 19, 20, and 27

Fig. 5 Concluded

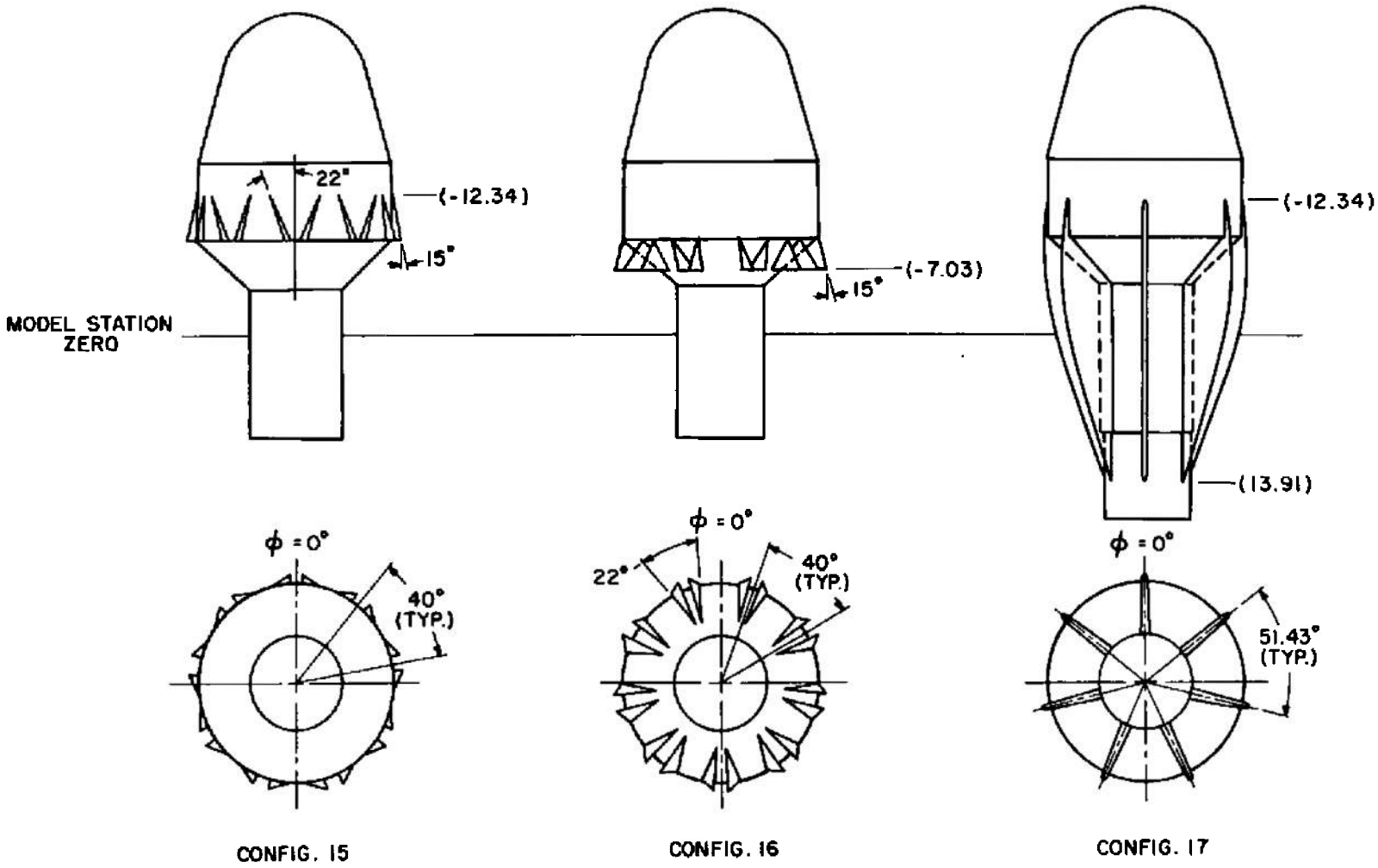

a. Configurations 15, 16, and 17

Fig. 6 Details of the Modifications to the Voyager Payloads

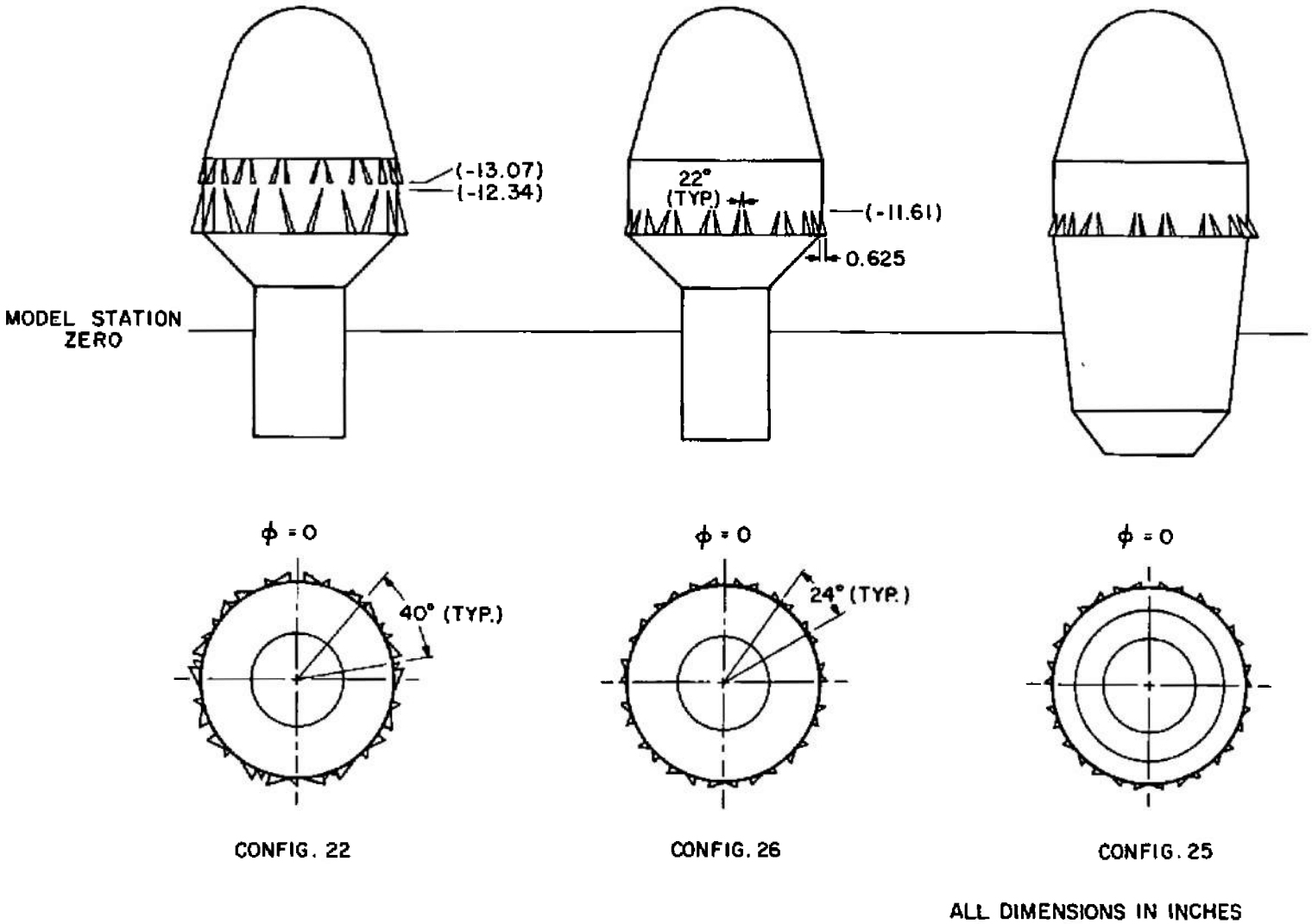

b. Configurations 22, 25, and 26

Fig. 6 Concluded

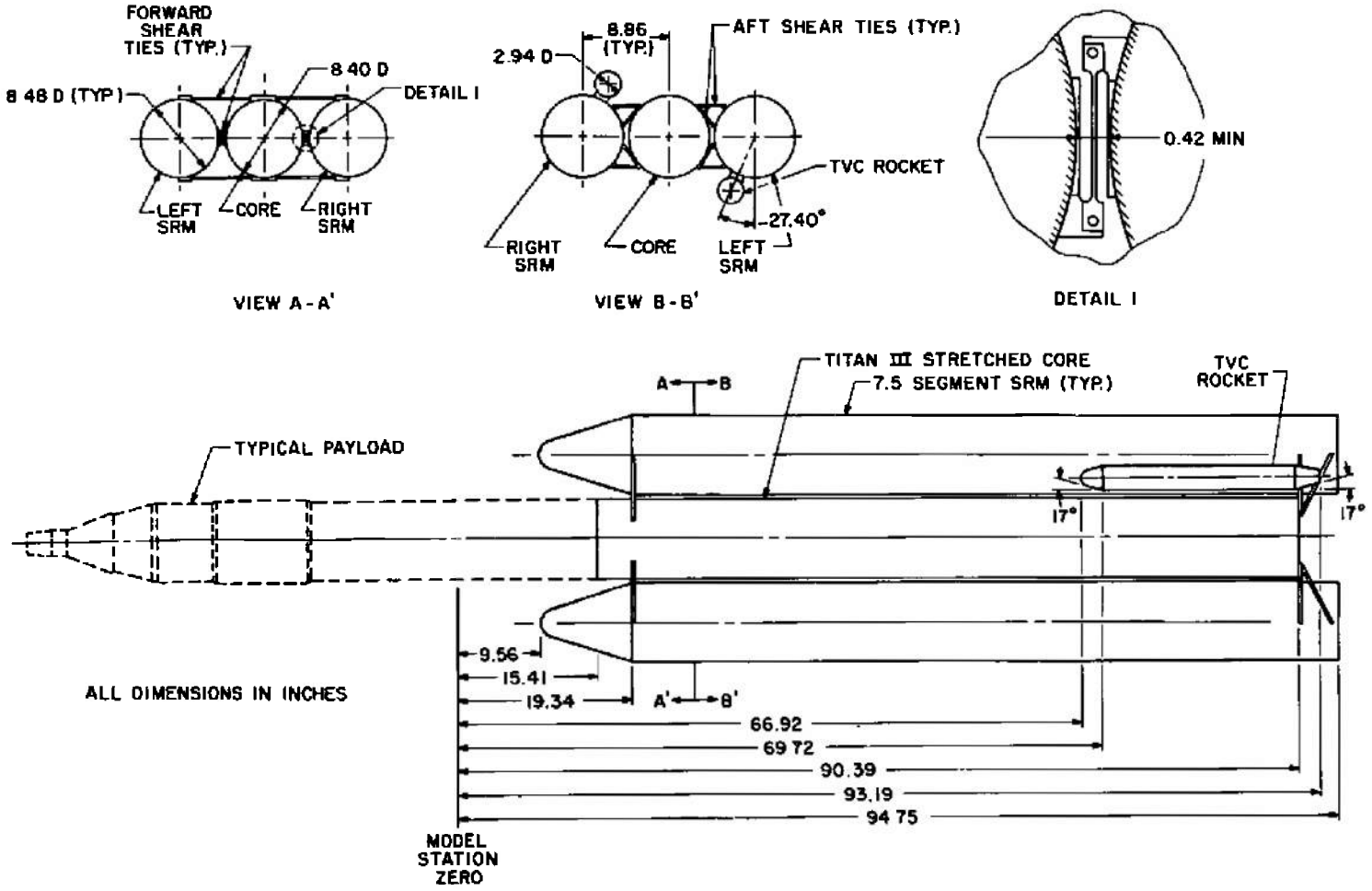

Fig. 7 Details of the Titan III Booster for the Phase III Test Configurations

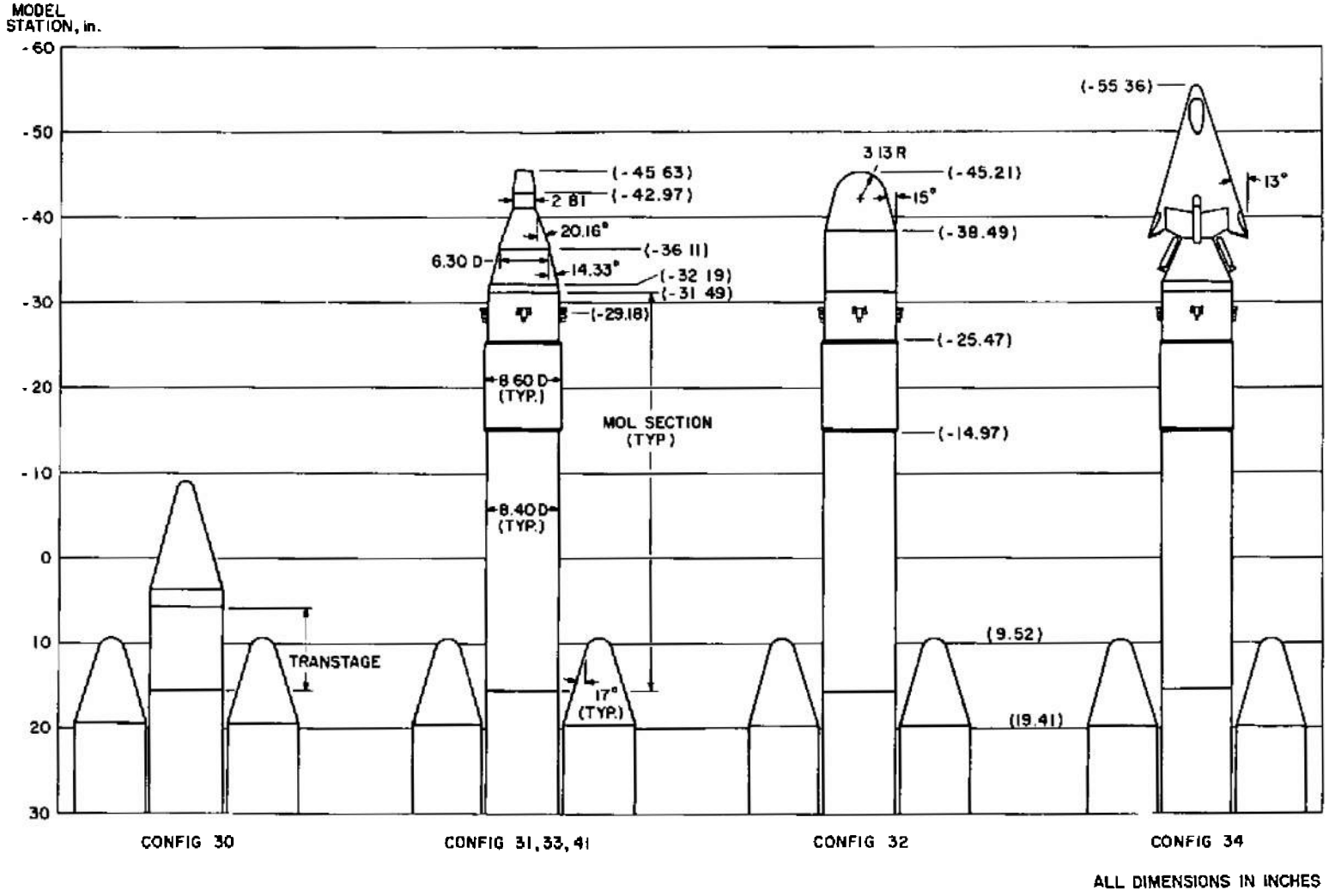

a. Configurations 30, 31, 32, 33, 34, and 41

Fig. 8 Details of the Payloads for the Phase III Test Configurations

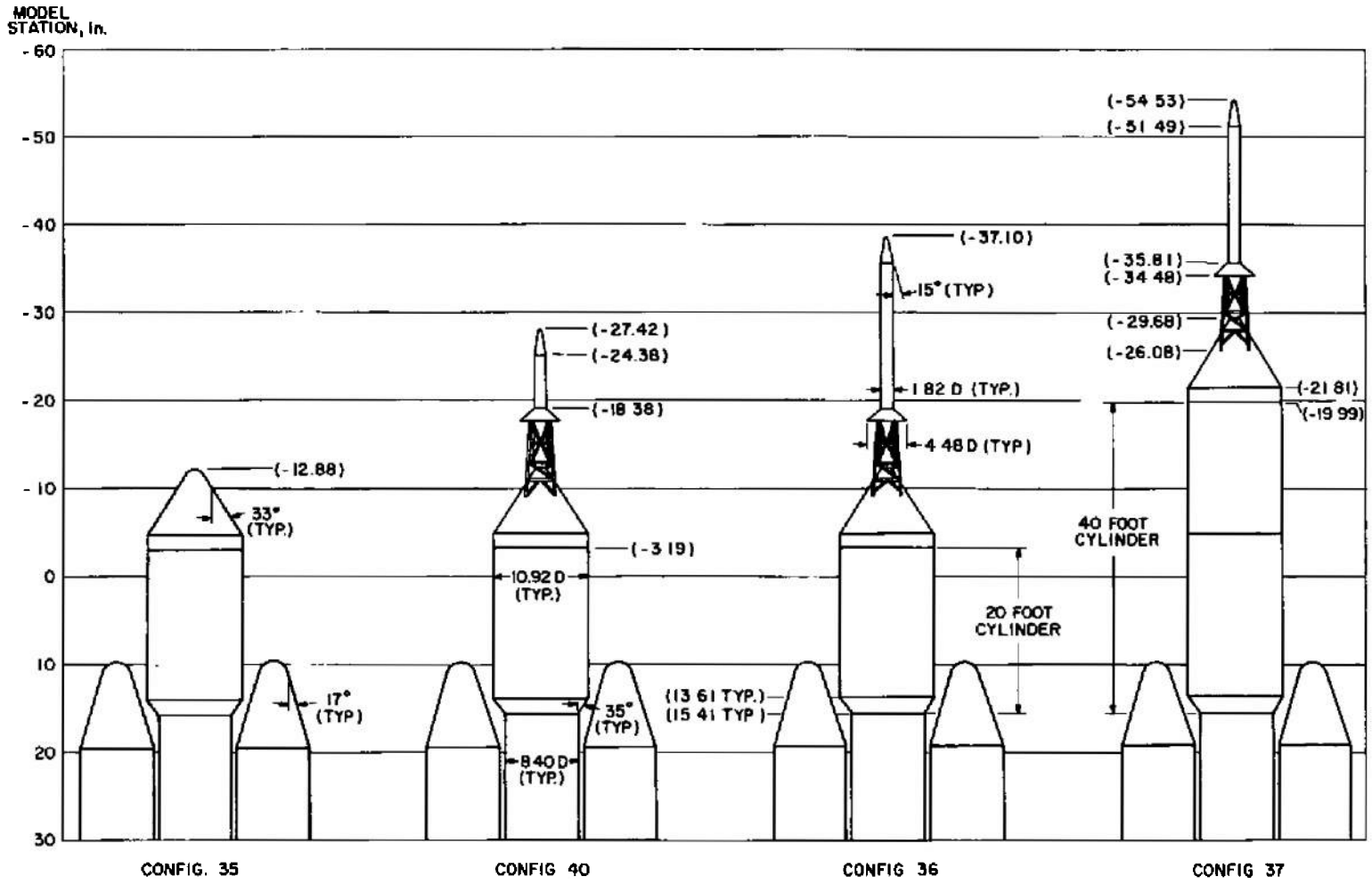

b. Configurations 35, 36, 37, and 40

Fig. 8 Concluded

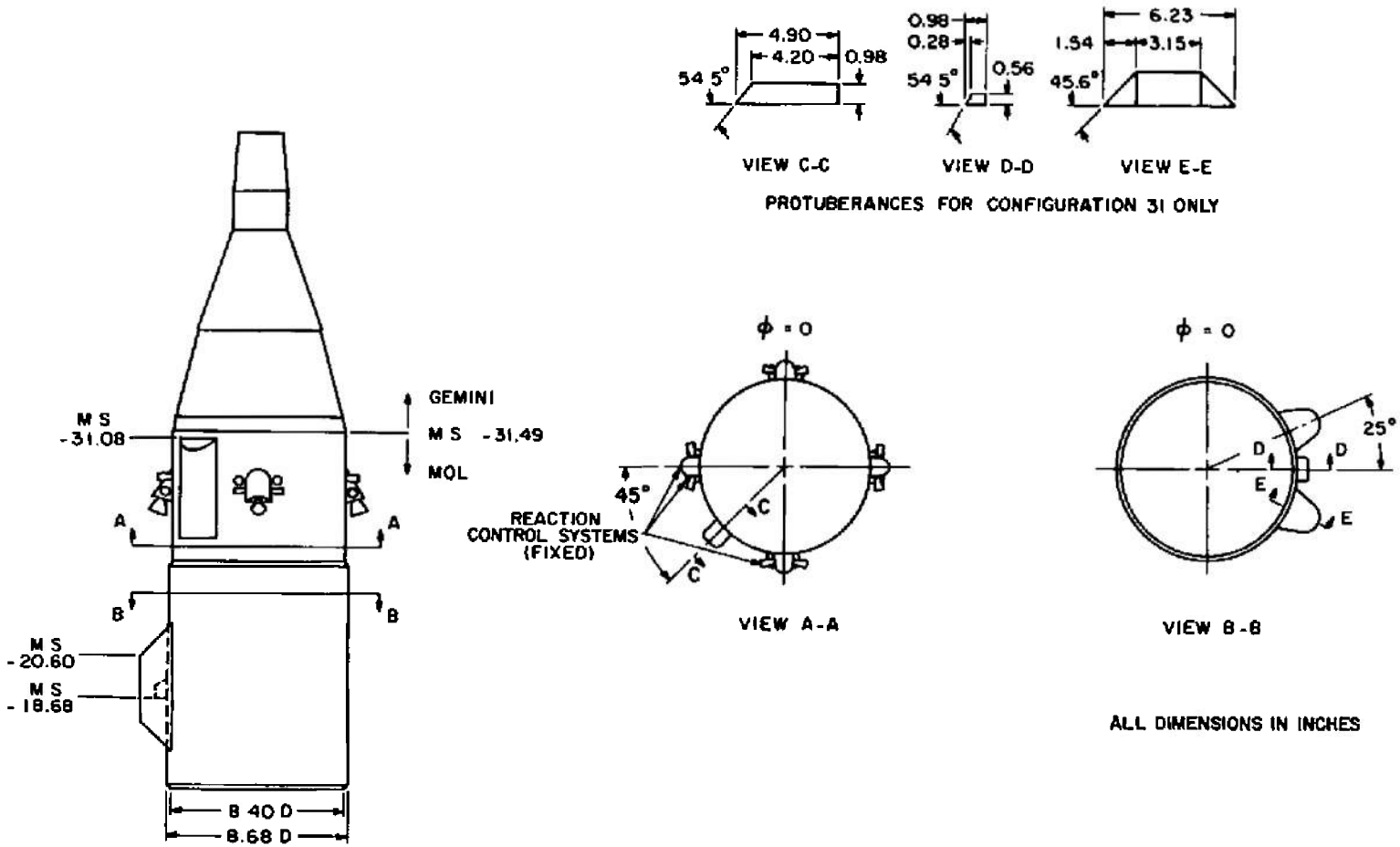

Fig. 9 Details of the Protuberances on the Phase III MOL Section

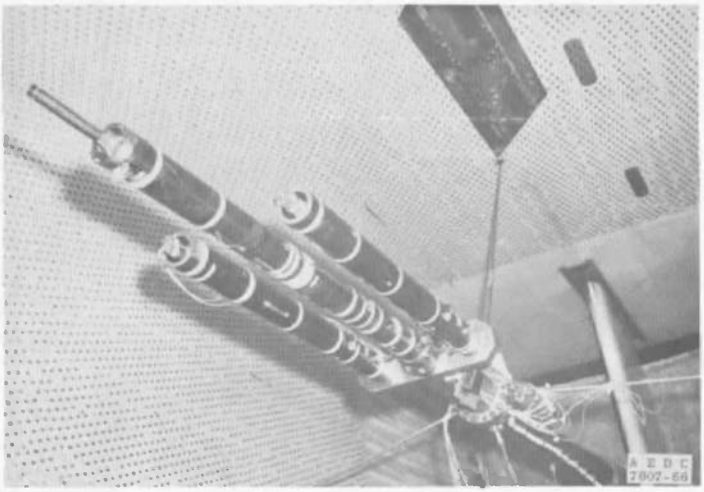

a. Sting Support System

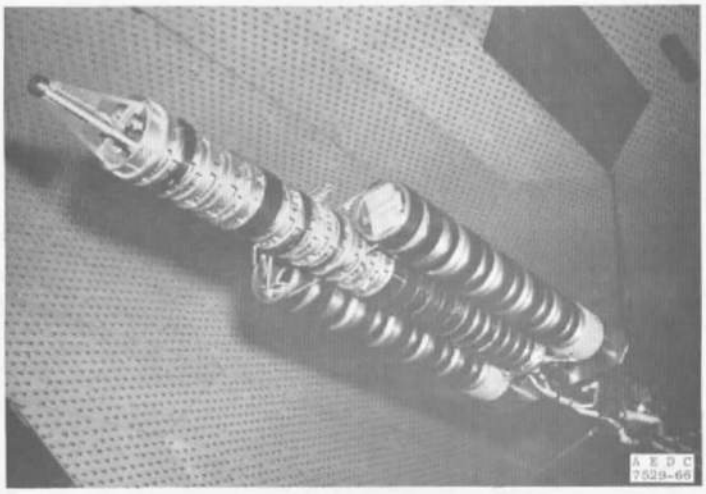

b. Elastic Structure with Concentrated Weights

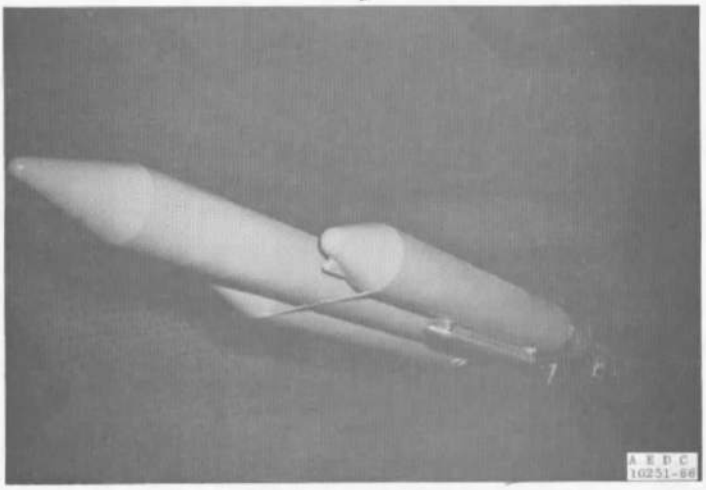

c. External Skin

Fig. 10 Photographs of the Model at Various Stages of Assembly

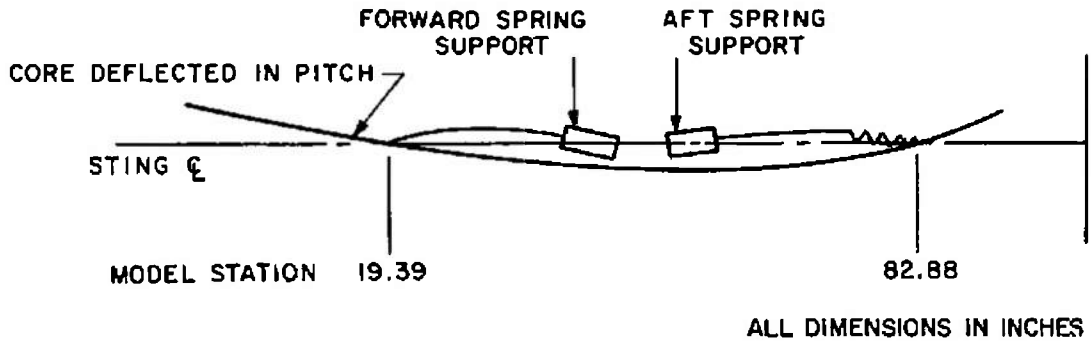

a. Side View

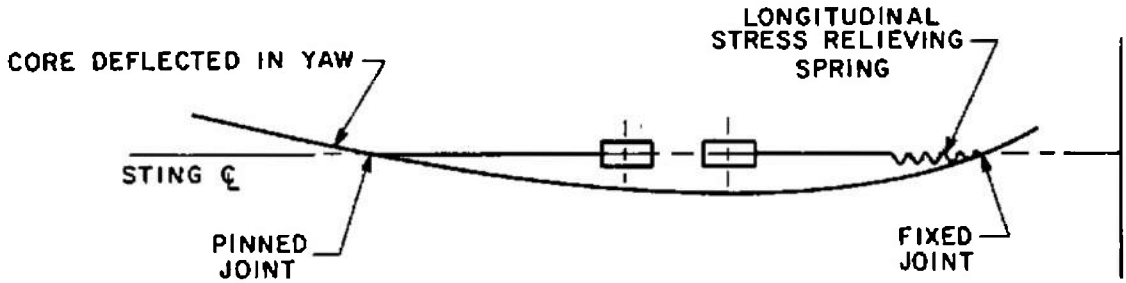

b. Top View

Fig. 11 Schematics of the Spring Support System for the Single-Body Configuration

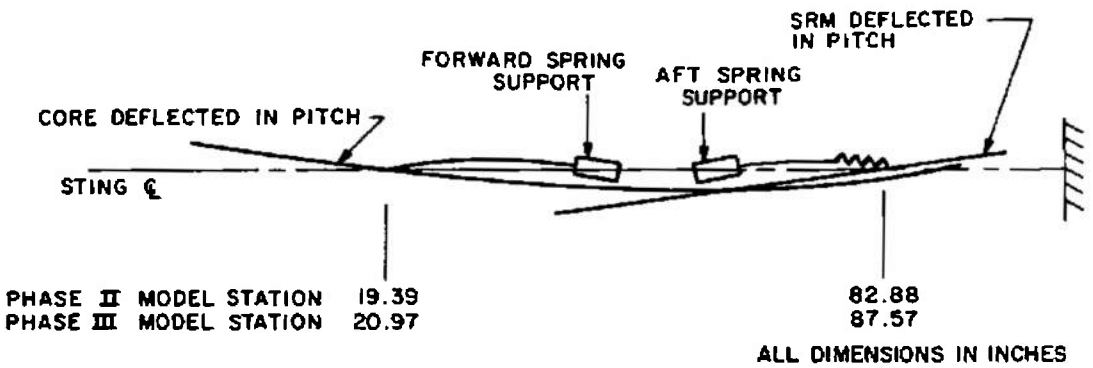

a. Side View

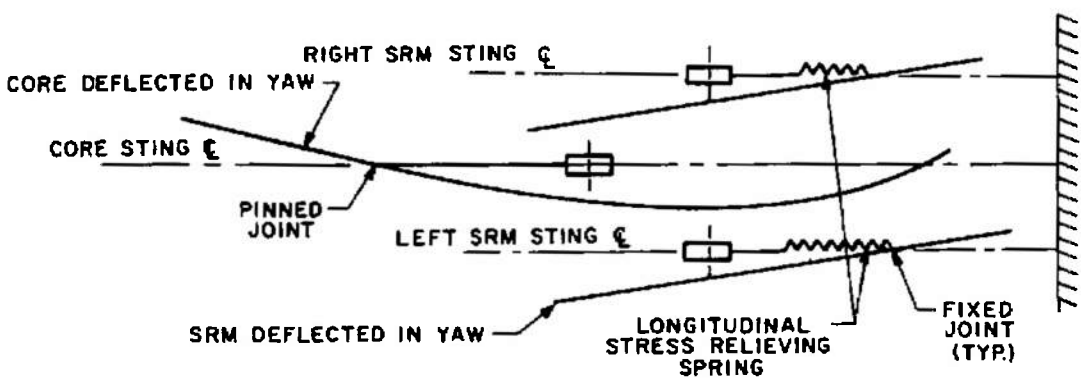

b. Top View

Fig. 12 Schematics of the Spring Support System for the Three-Body Configurations

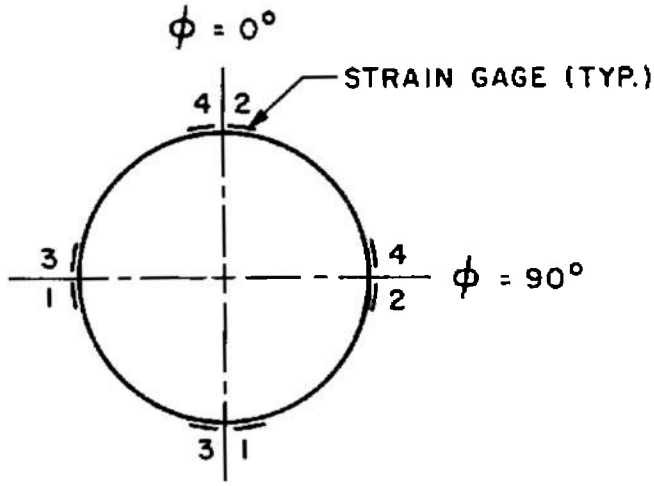

TYPICAL CORE CROSS SECTION

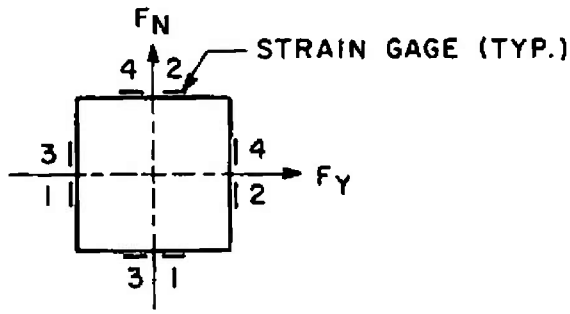

TYPICAL SUPPORT SPRING CROSS SECTION

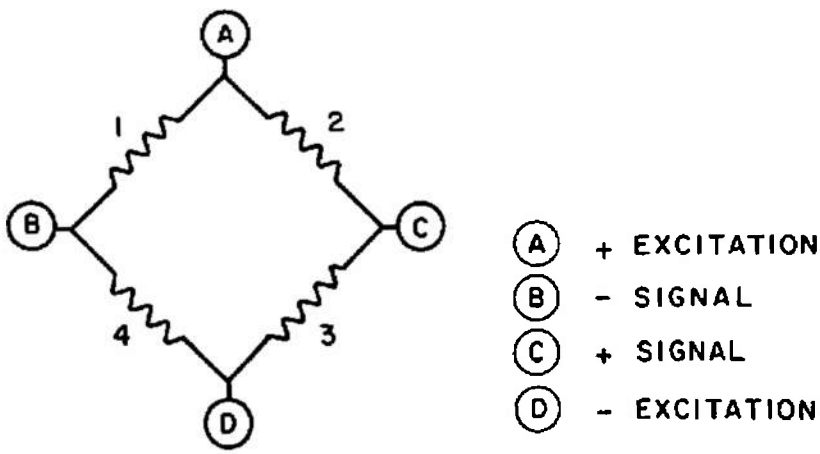

TYPICAL SENSOR

Fig. 13 Details of the Bending-Moment and Force Sensors

BENDING-MOMENT SENSOR LOCATIONS	
SENSOR	MODEL STATION
M_{P1} , M_{Y1}	18.55
M_{P2} , M_{Y2}	24.50
M_{P3} , M_{Y3}	30.65
M_{P4} , M_{Y4}	33.75
M_{P5} , M_{Y5}	38.20
M_{P6} , M_{Y6}	44.40
M_{P7} , M_{Y7}	52.25
M_{P8} , M_{Y8}	59.75
M_{P9} , M_{Y9}	70.80

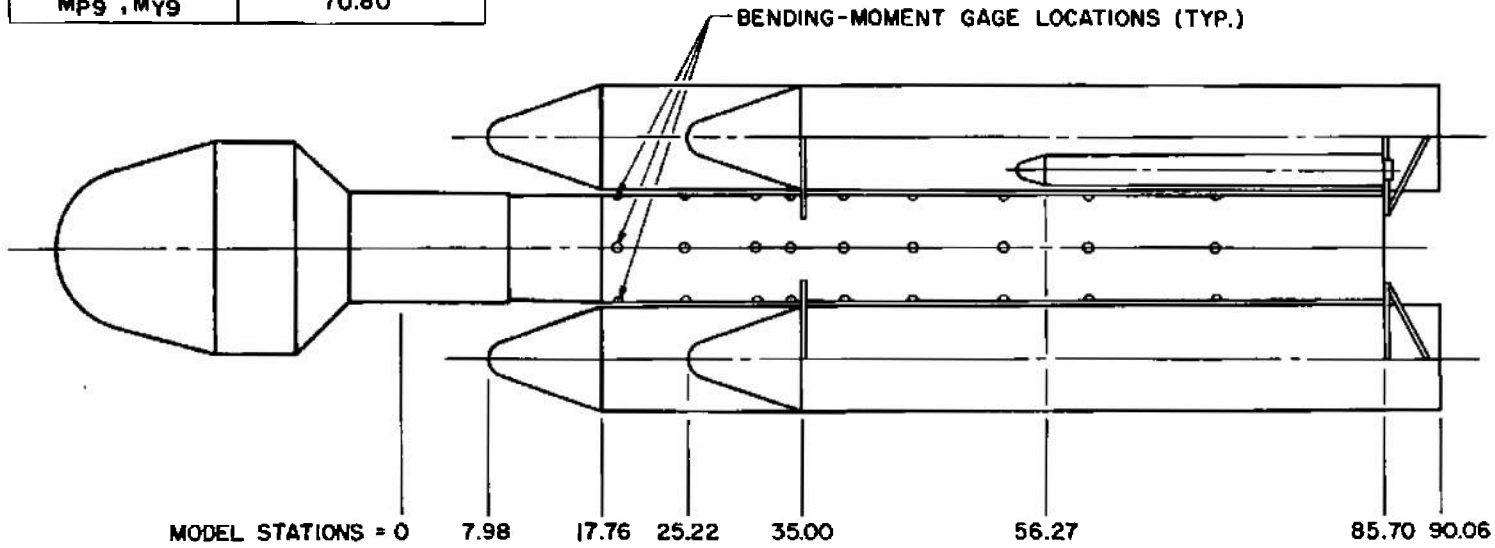

ALL DIMENSIONS IN INCHES

a. Phase II Test Configurations

Fig. 14 Axial Locations of the Bending-Moment Sensors

BENDING-MOMENT SENSOR LOCATIONS	
SENSOR	MODEL STATION
M_{P1} , M_{Y1}	- 13.84
M_{P2} , M_{Y2}	6.86
M_{P3} , M_{Y3}	20.16
M_{P4} , M_{Y4}	21.41
M_{P5} , M_{Y5}	23.16
M_{P6} , M_{Y6}	33.73
M_{P7} , M_{Y7}	35.48
M_{P8} , M_{Y8}	51.98
M_{P9} , M_{Y9}	53.98
M_{P10}, M_{Y10}	55.36
M_{P11}, M_{Y11}	69.41
M_{P12}, M_{Y12}	70.73

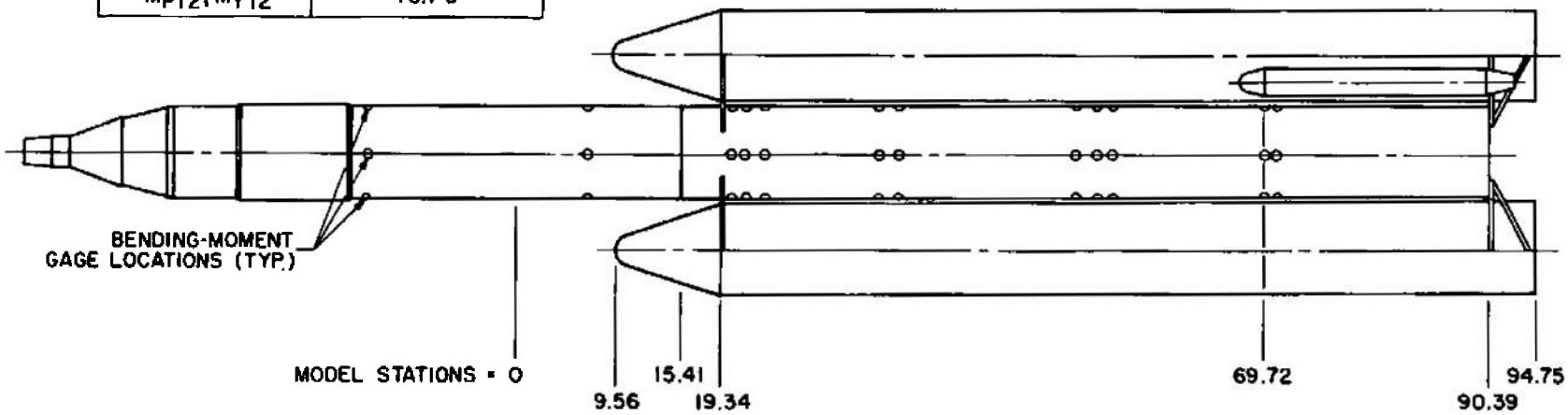

ALL DIMENSIONS IN INCHES

b. Phase III Test Configurations

Fig. 14 Concluded

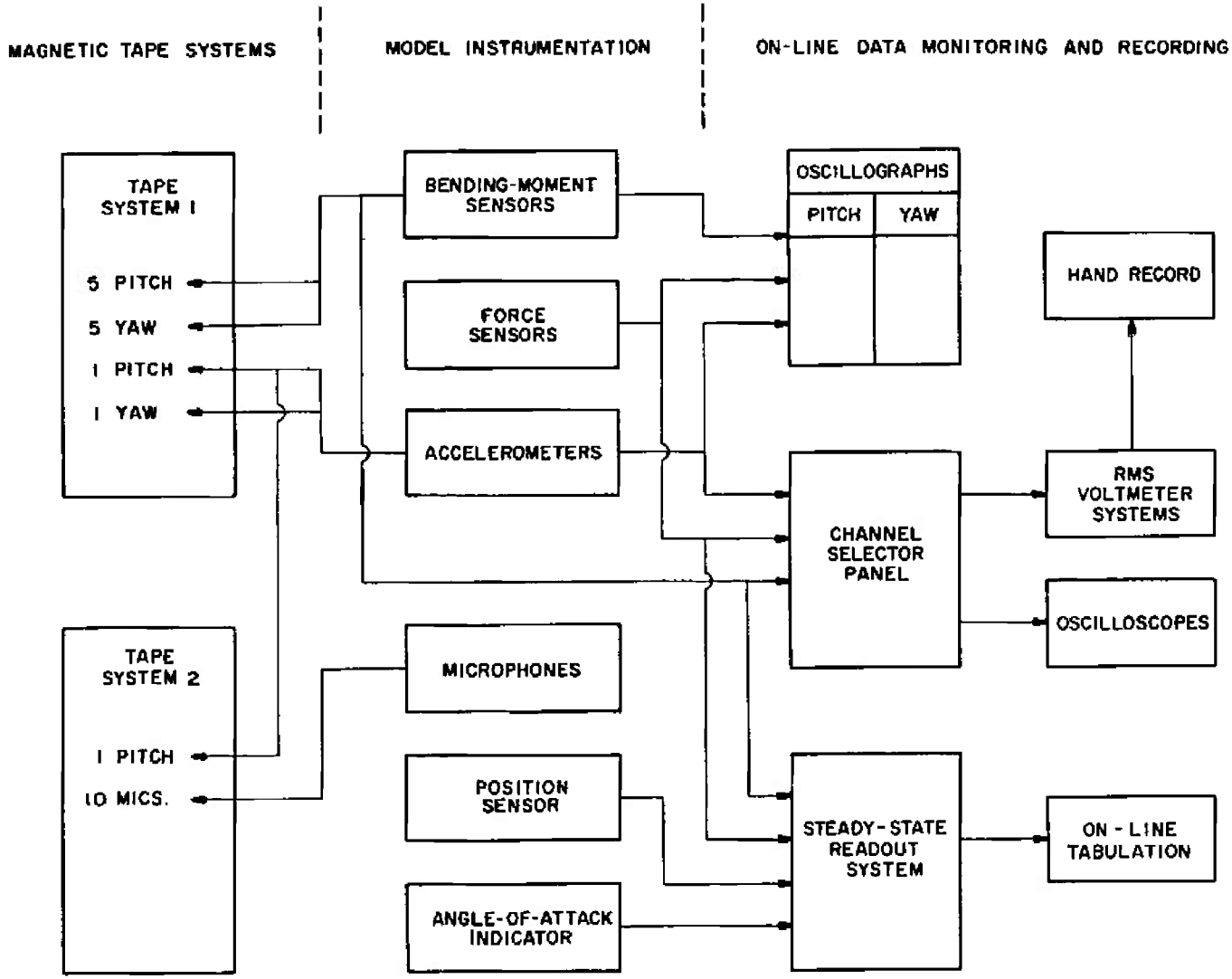

Fig. 15 Data Acquisition System

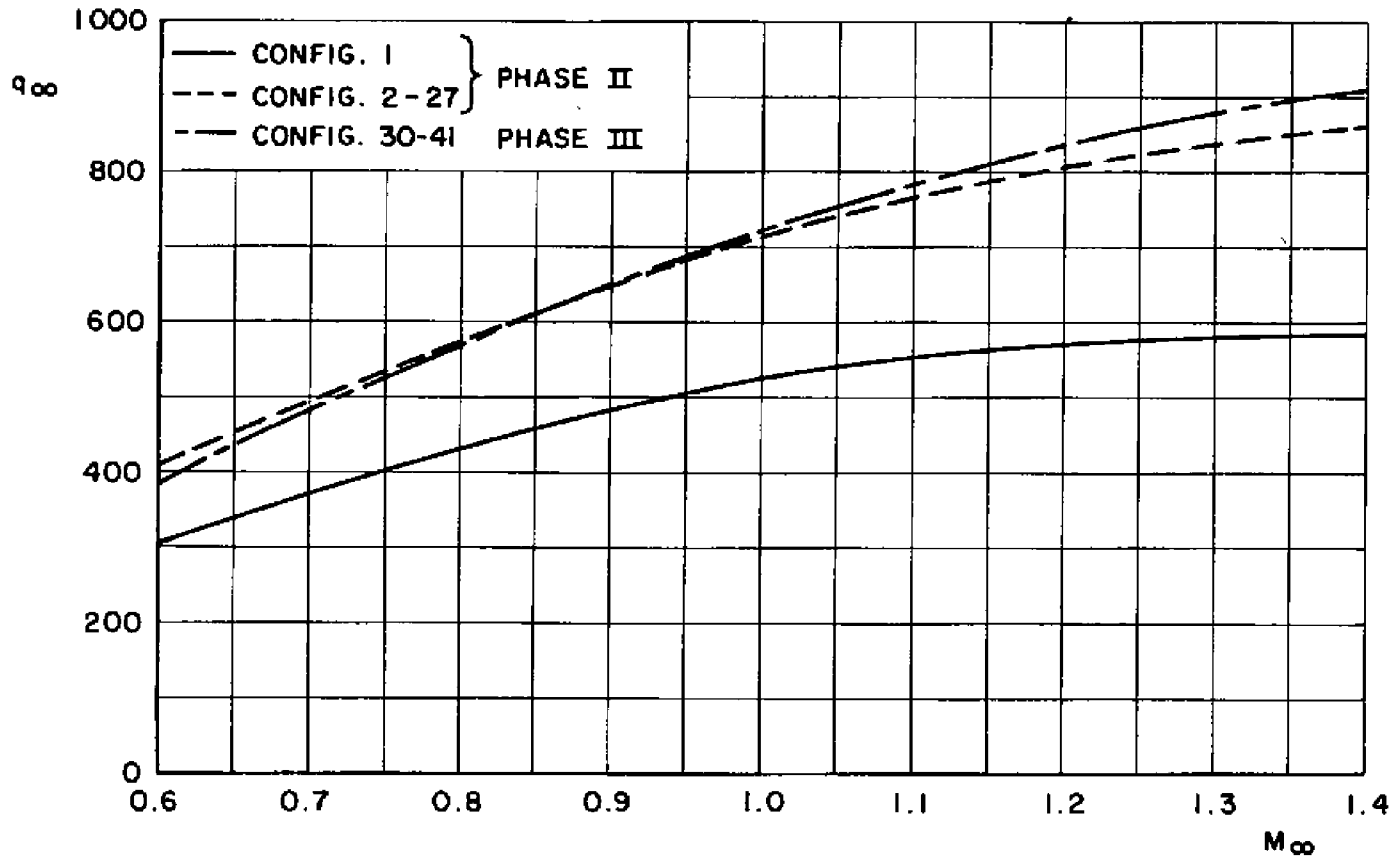

Fig. 16 Variation of Dynamic Pressure with Mach Number for Normal Test Conditions

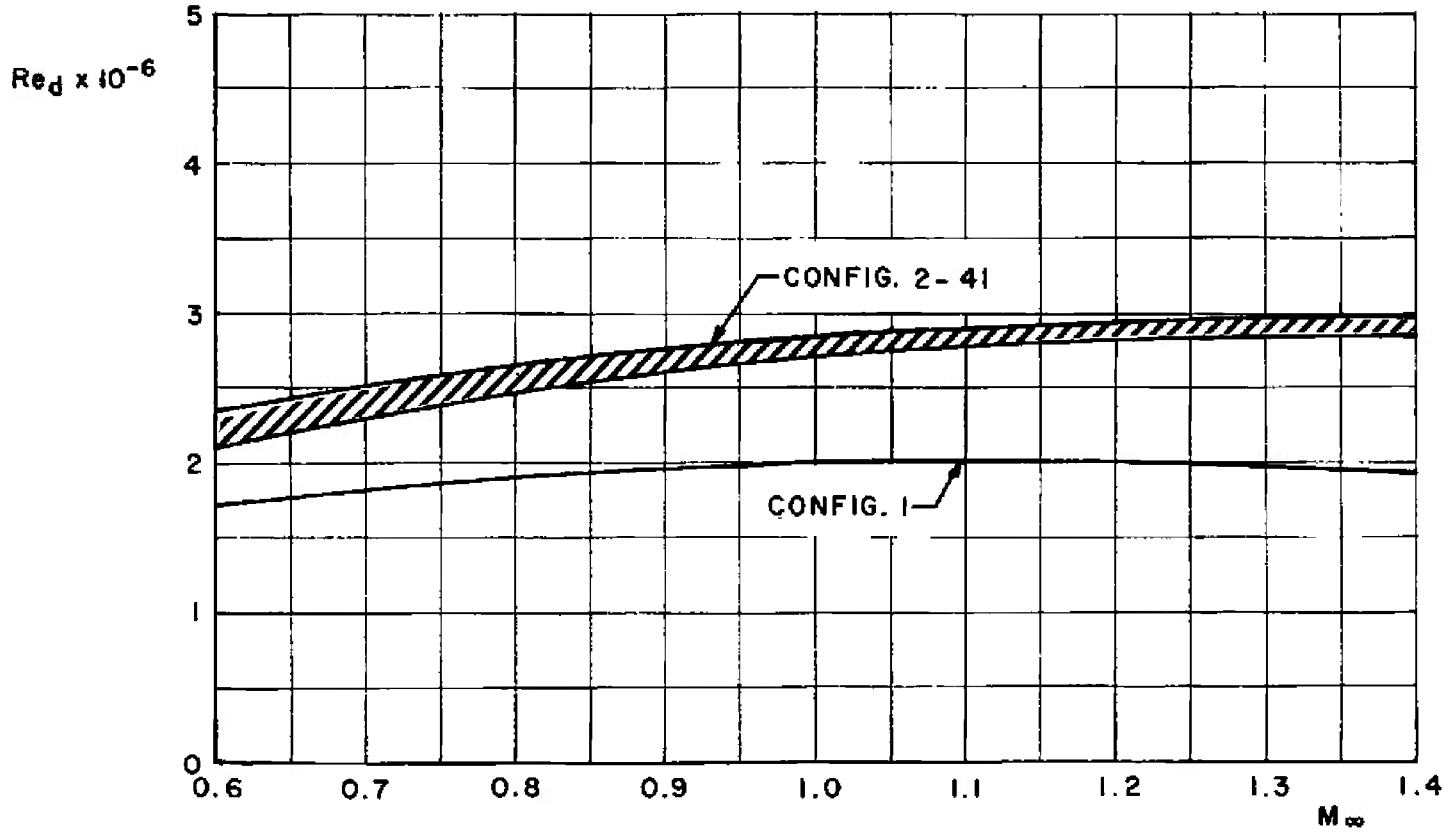

Fig. 17 Variation of Reynolds Number with Mach Number for Normal Test Conditions

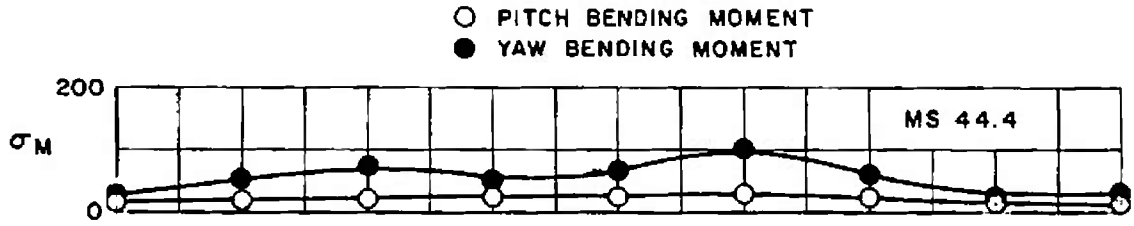

a. Configuration 1

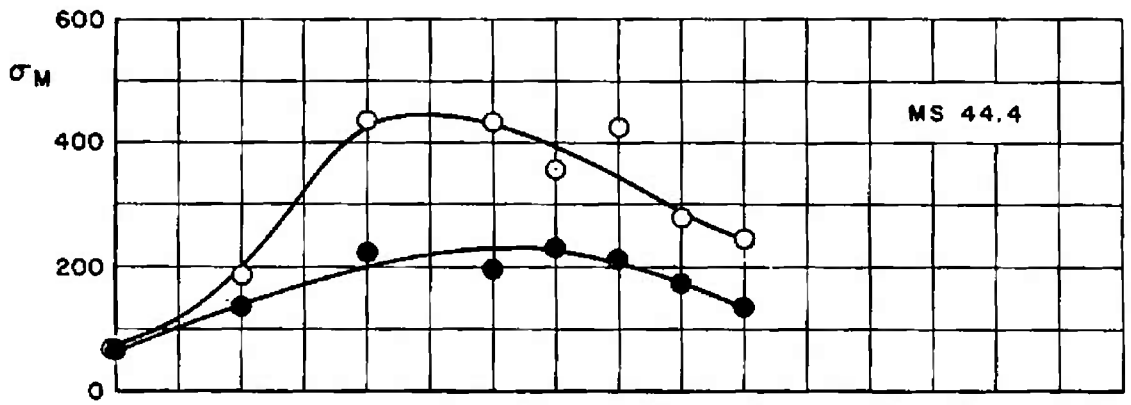

b. Configuration 2

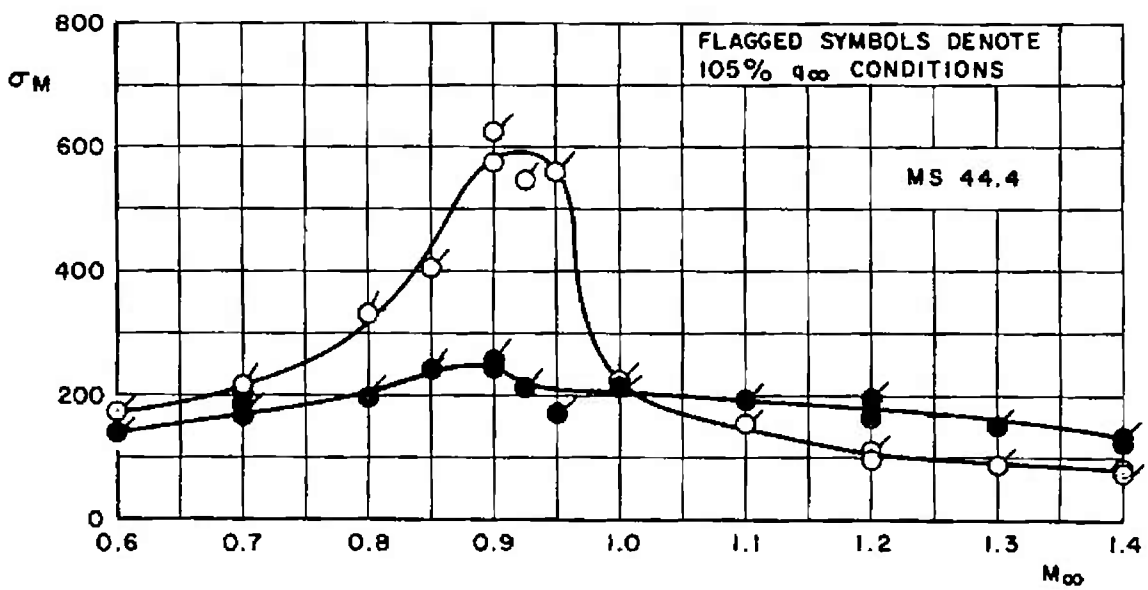

c. Configuration 9

Fig. 18 Variations of the Total Elastic RMS Bending Moment with Mach Number, Phase II Test

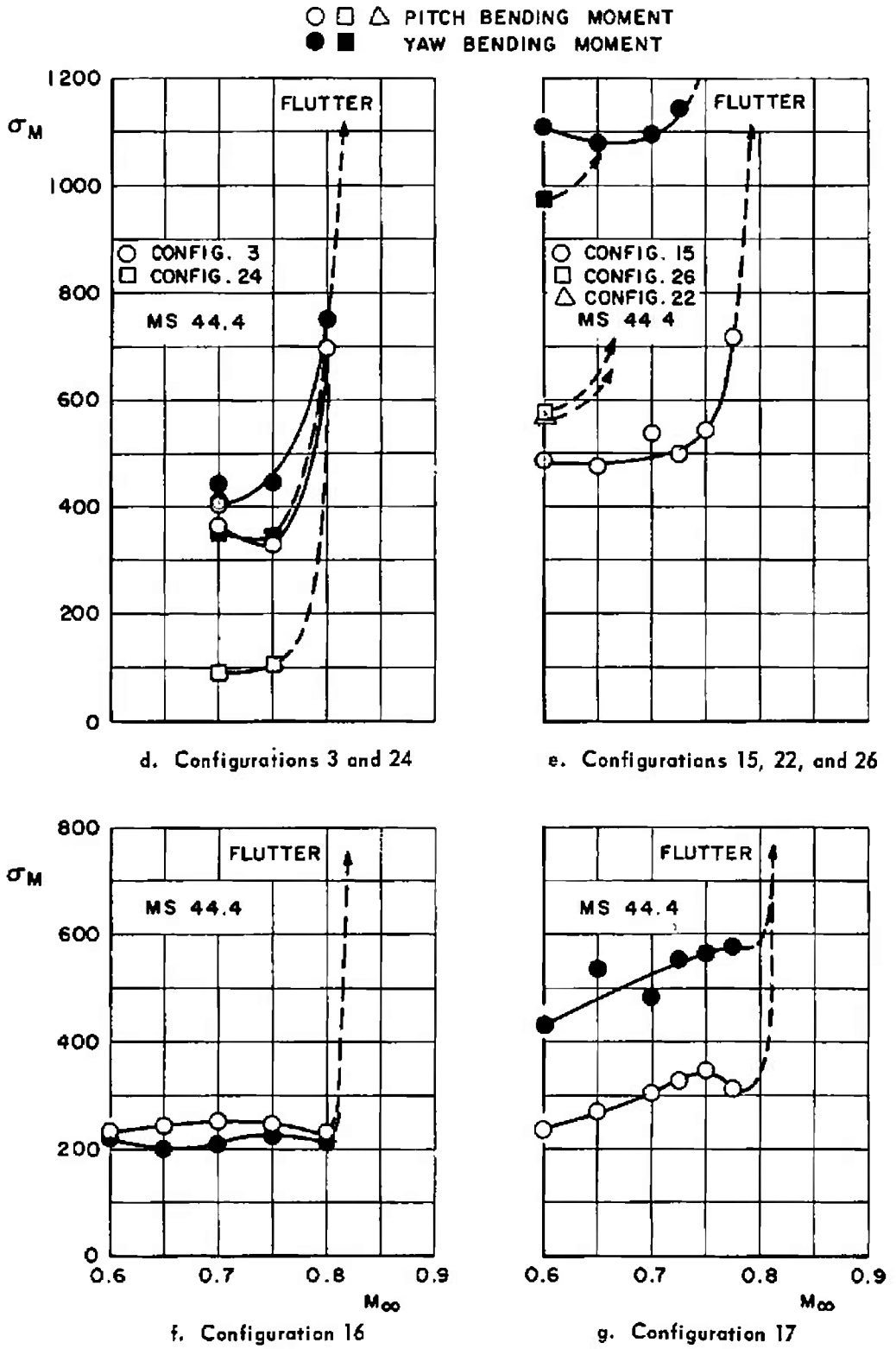

d. Configurations 3 and 24

e. Configurations 15, 22, and 26

f. Configuration 16

g. Configuration 17

Fig. 18 Continued

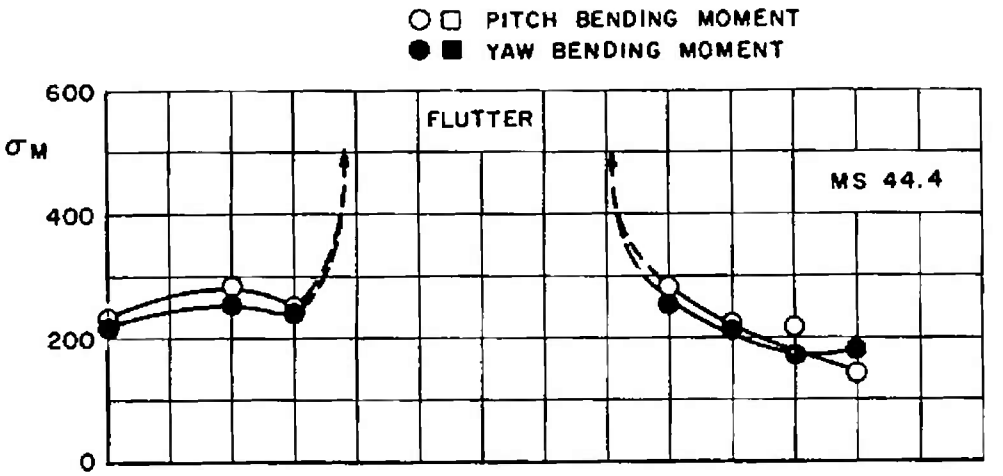

h. Configuration 4

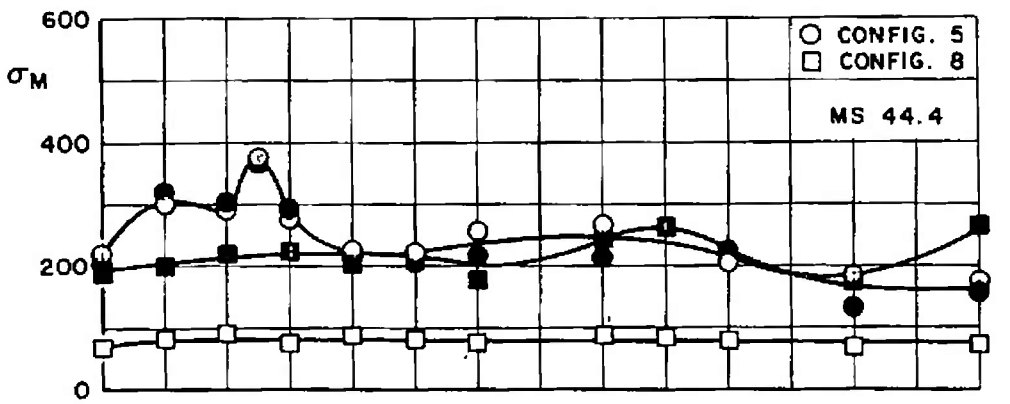

i. Configurations 5 and 8

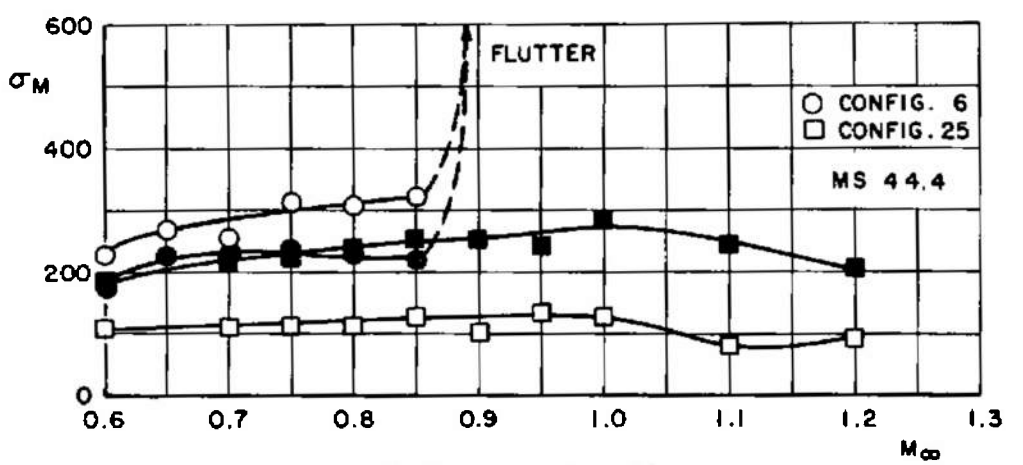

j. Configurations 6 and 25

Fig. 18 Continued

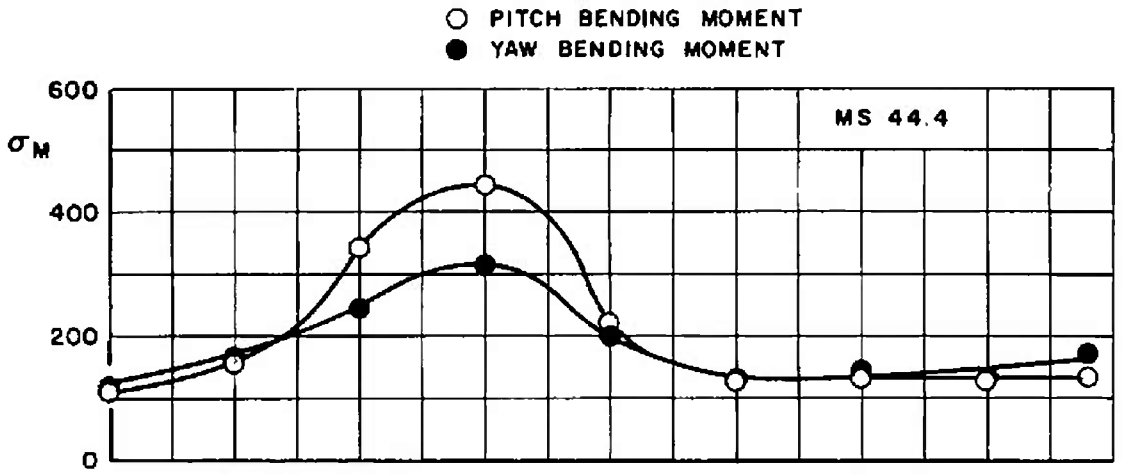

k. Configuration 19

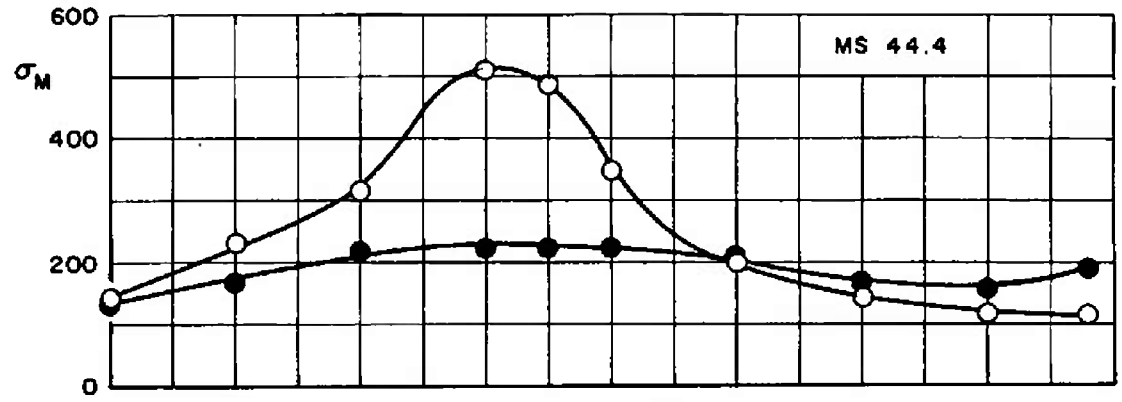

l. Configuration 20

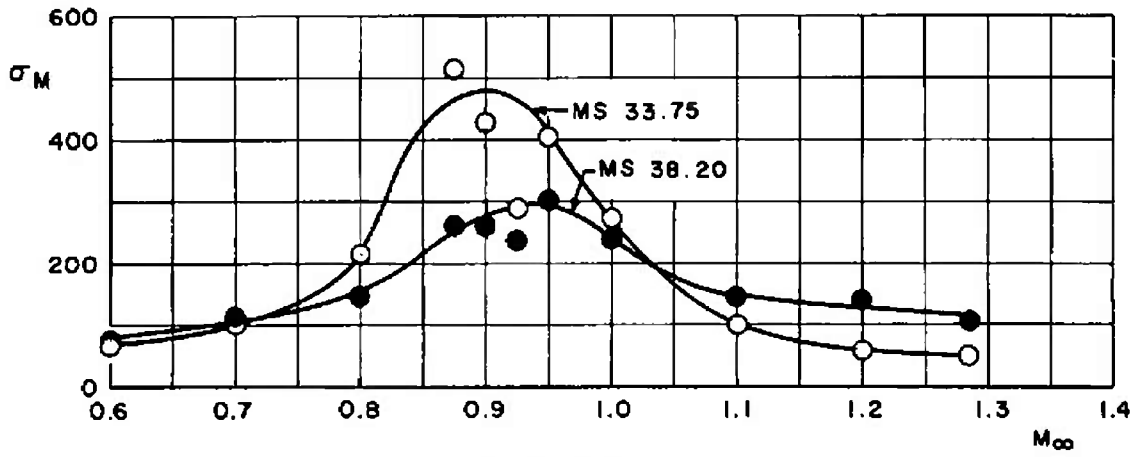

m. Configuration 27

Fig. 18 Concluded

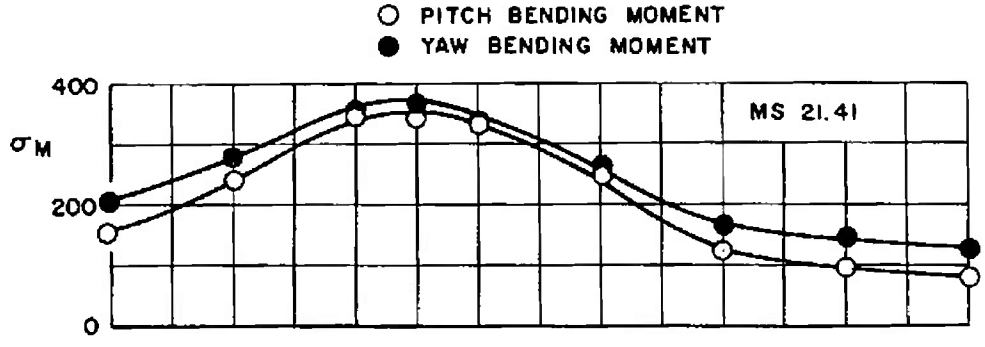

a. Configuration 30

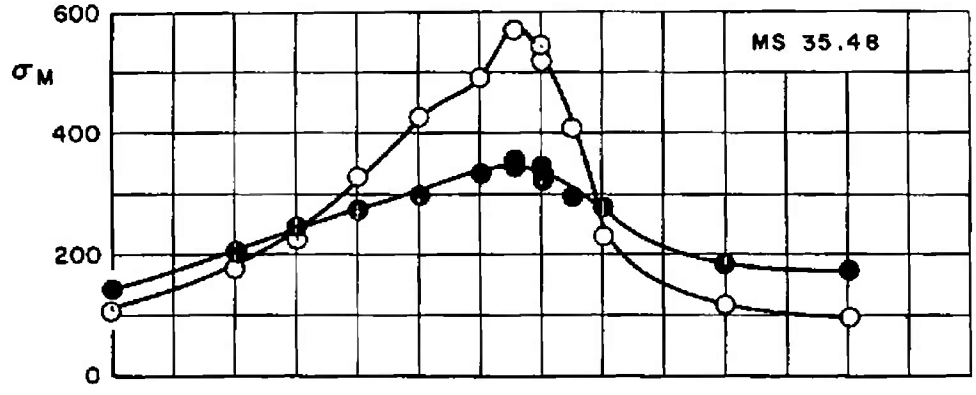

b. Configuration 31

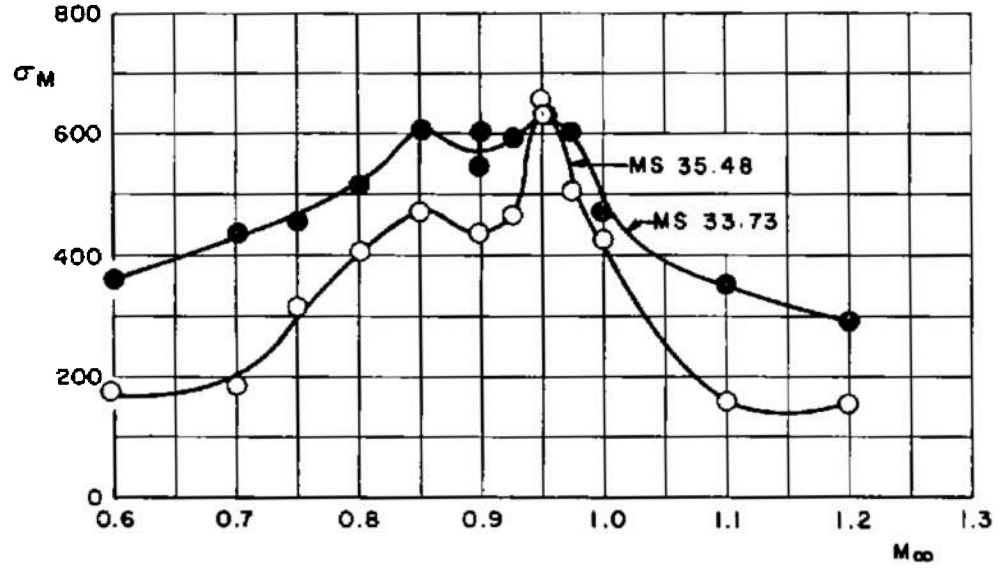

c. Configuration 32

Fig. 19 Variations of the Total Elastic RMS Bending Moment with Mach Number, Phase III Test

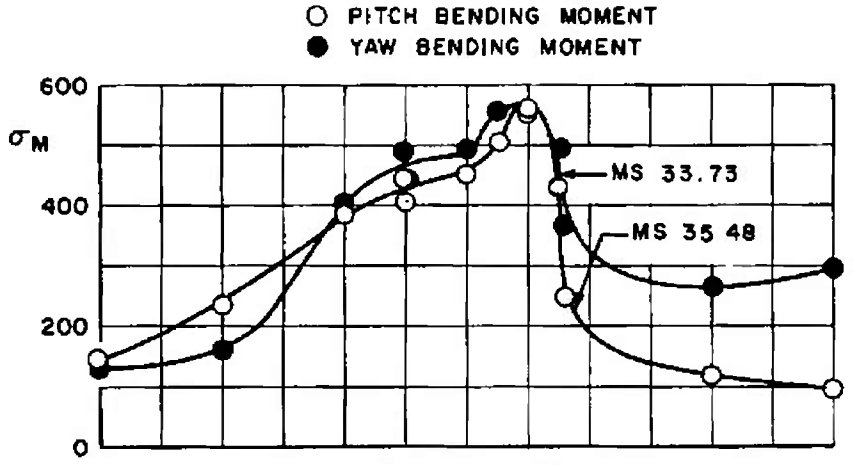

d. Configuration 33

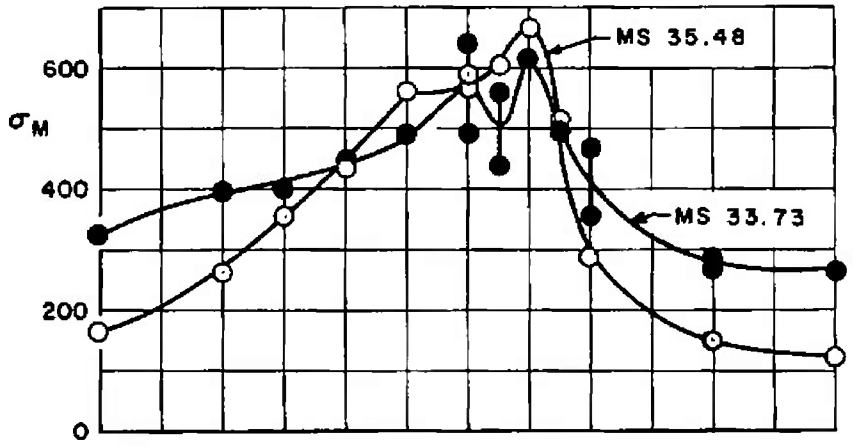

e. Configuration 41

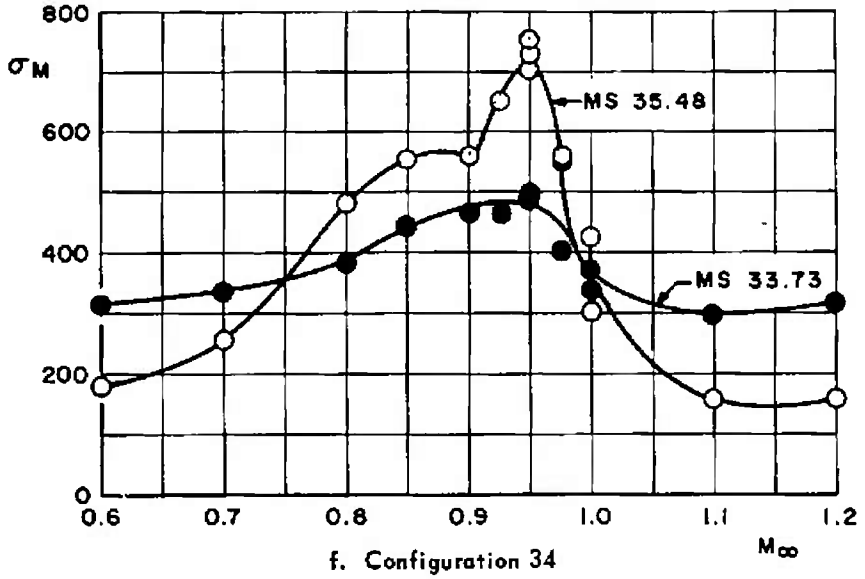

f. Configuration 34

Fig. 19 Continued

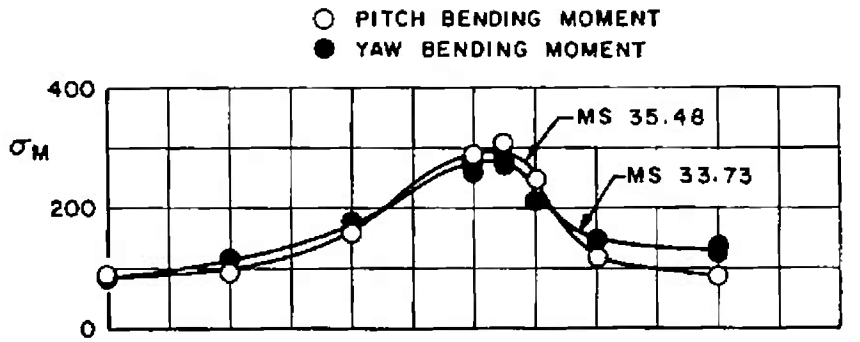

g. Configuration 35

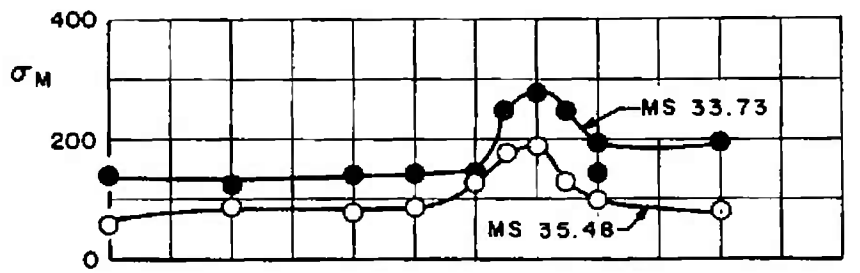

h. Configuration 36

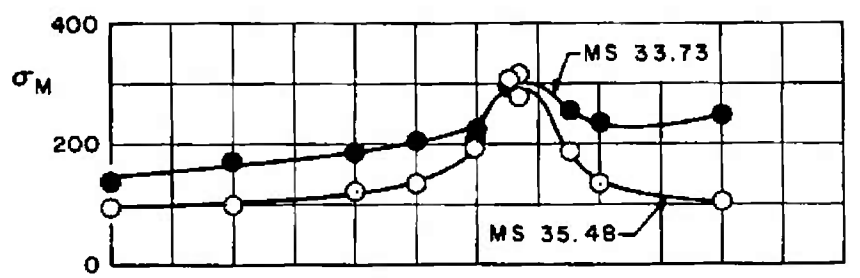

i. Configuration 37

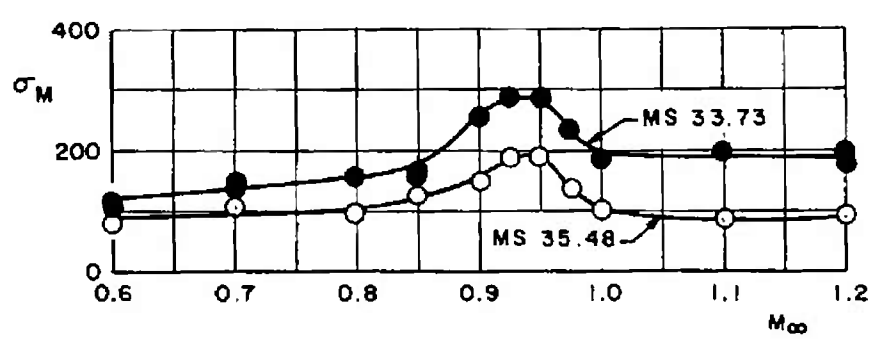

j. Configuration 40

Fig. 19 Concluded

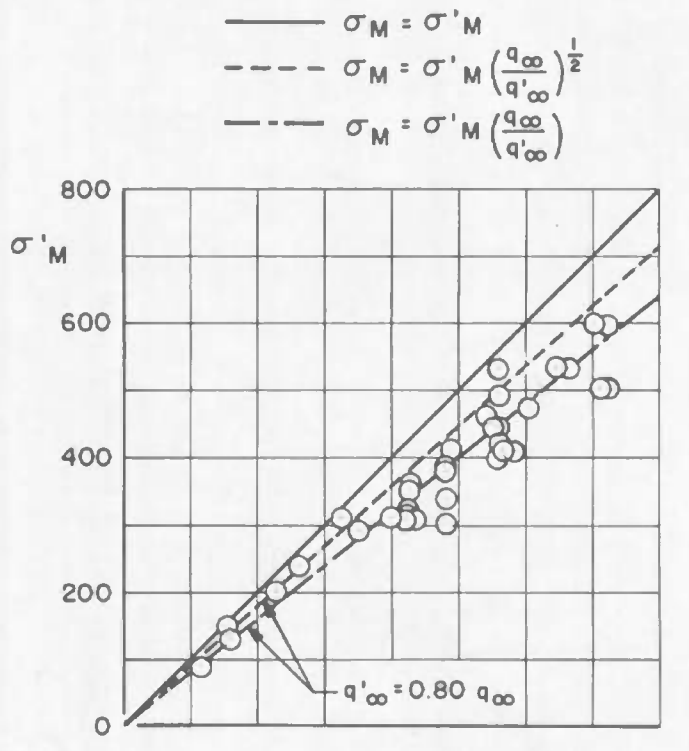

a. Pitch

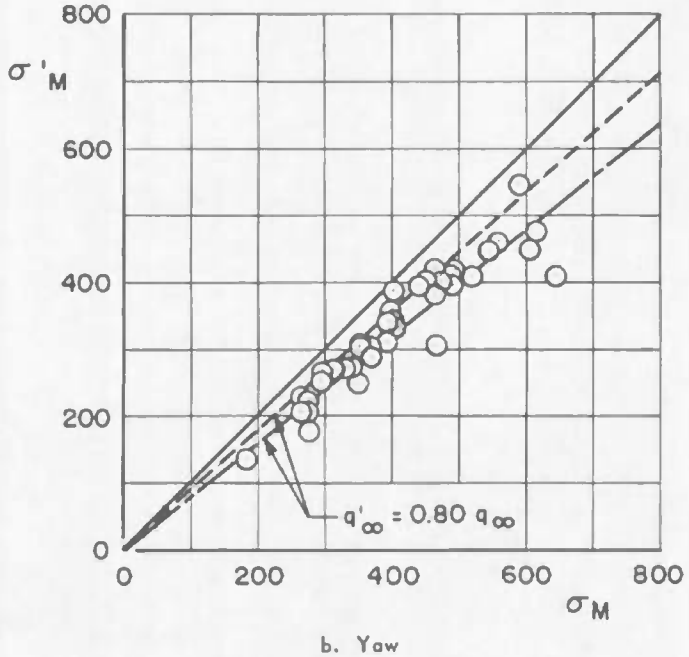

b. Yaw

Fig. 20 Effect of Dynomic Pressure on the Total Elostic RMS Bending Moment, Phase III MOL Configuratians

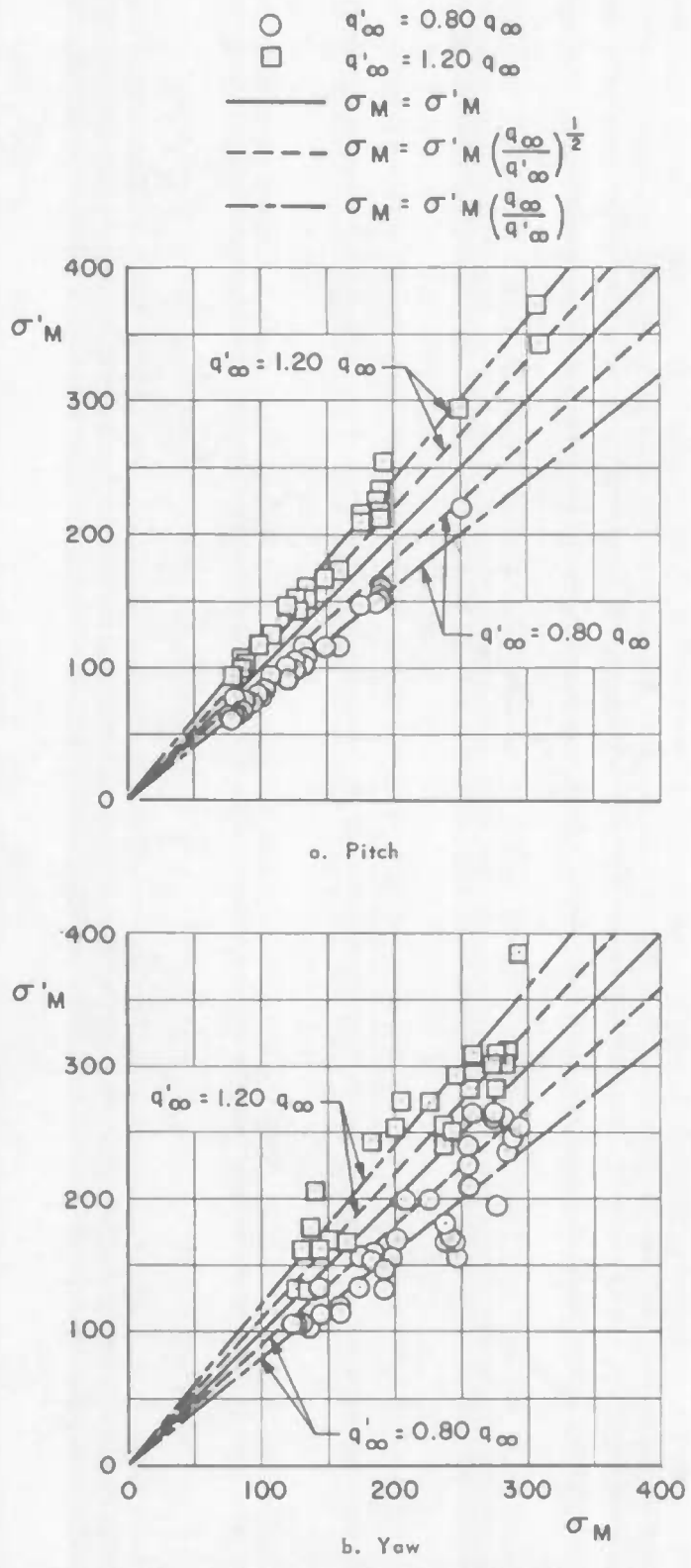

Fig. 21 Effects of Dynamic Pressure on the Total Elastic RMS Bending Moment, Phase III Apollo Configurations

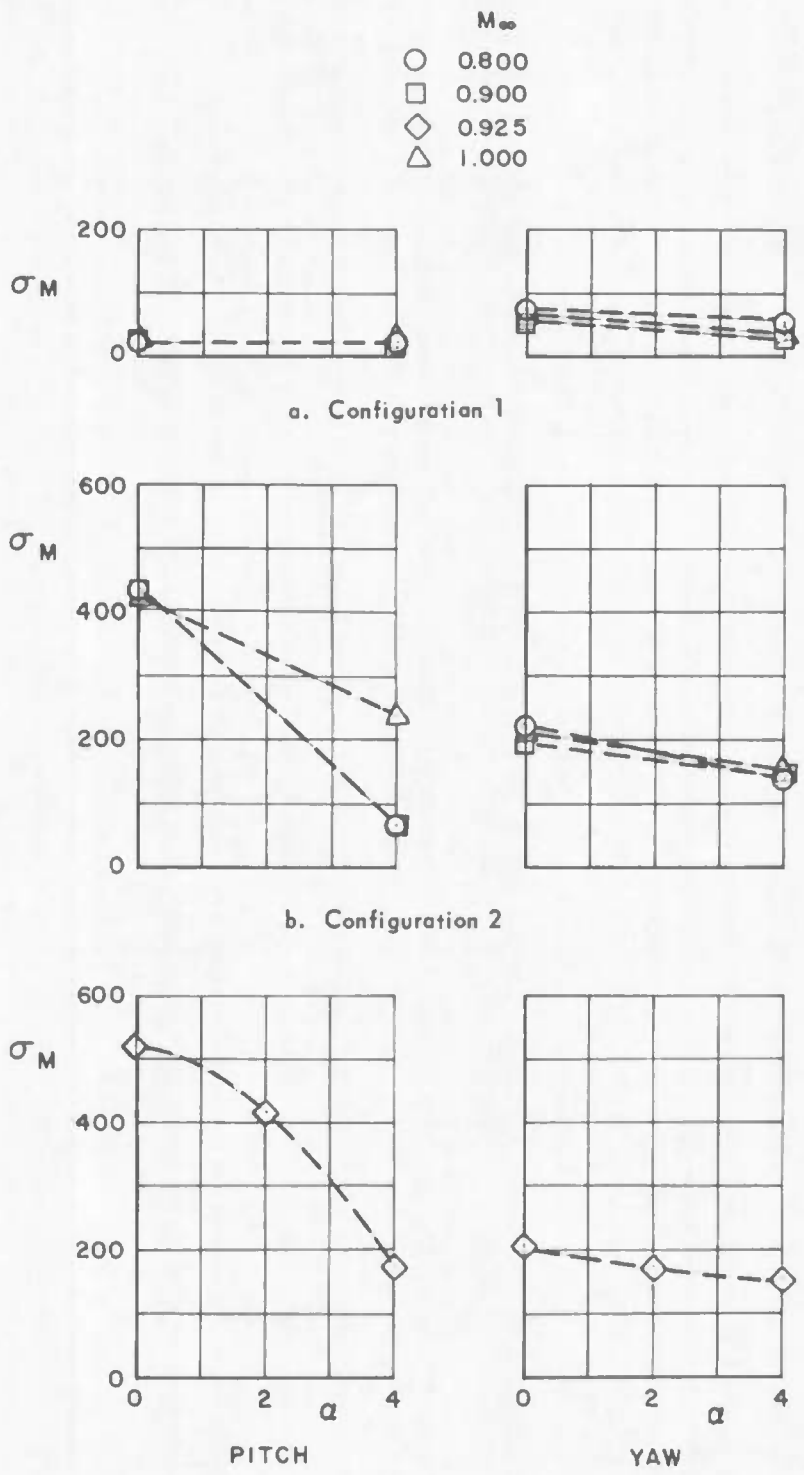

a. Configuratian 1

b. Configuration 2

c. Canfiguratian 9

Fig. 22 Variatian af the Total Elastic RMS Bending Moment with Angle of Attack, Pitch and Yaw, Phase II Test

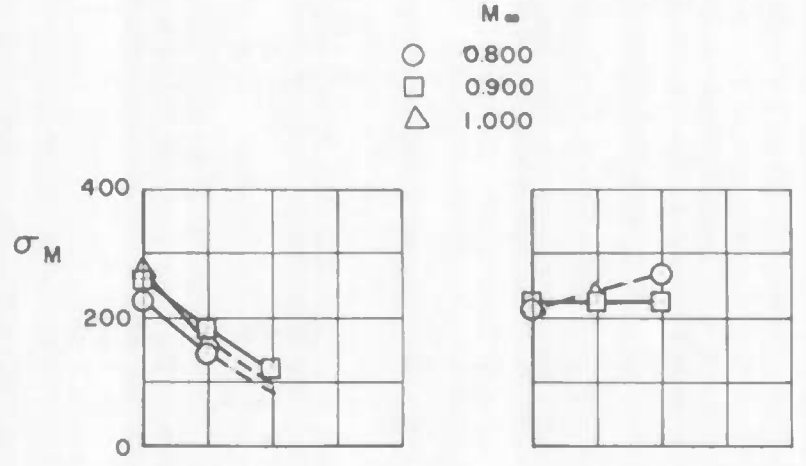

d. Configuration 5

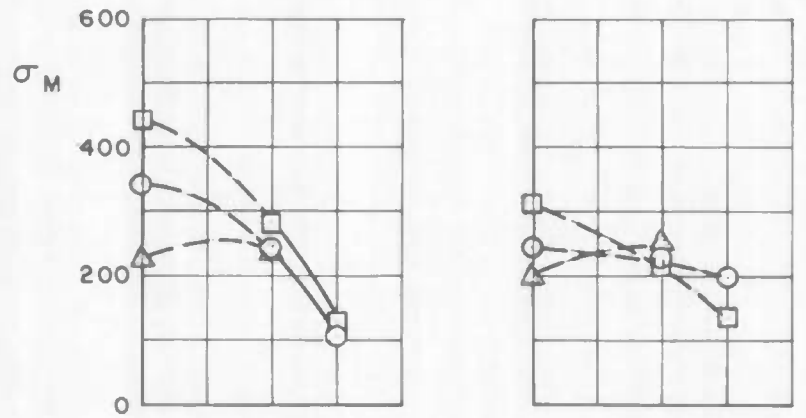

e. Configuration 19

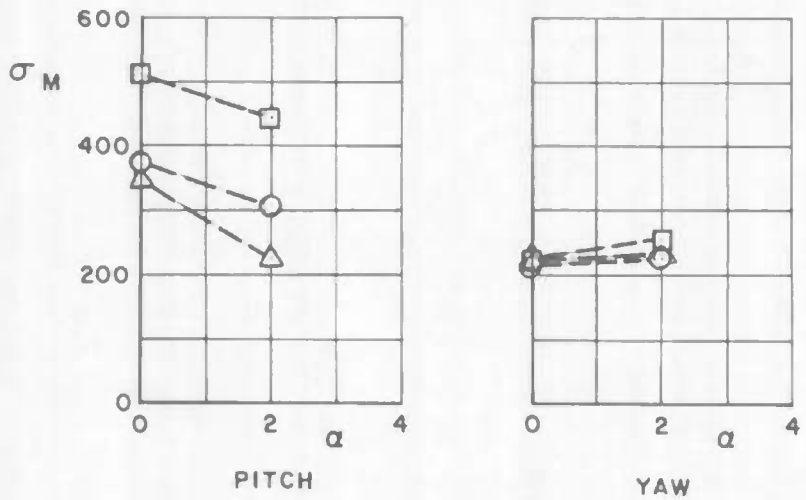

f. Configuration 20

Fig. 22 Concluded

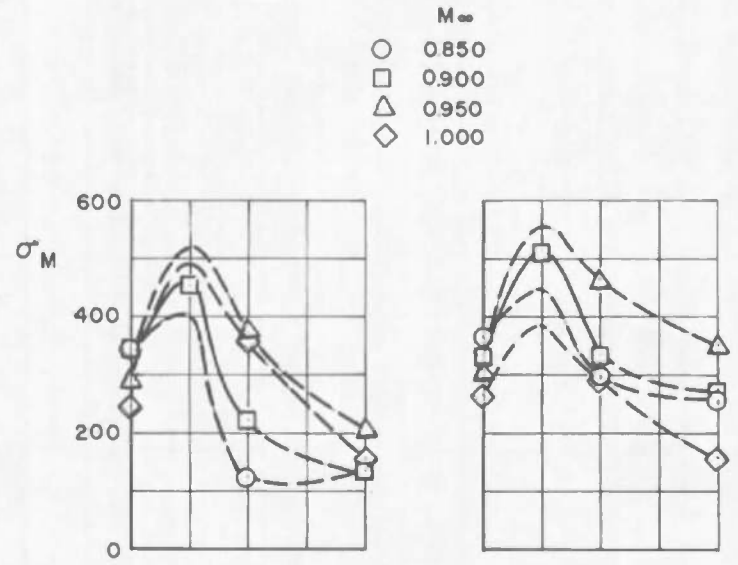

a. Configurotion 30

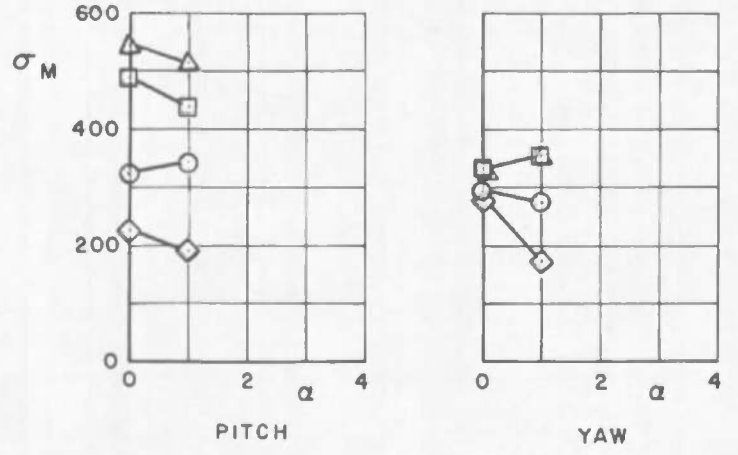

b. Configuration 31

Fig. 23 Variation of the Total Elastic RMS Bending Moment with Angle of Attack, Pitch and Yaw, Phase III Test

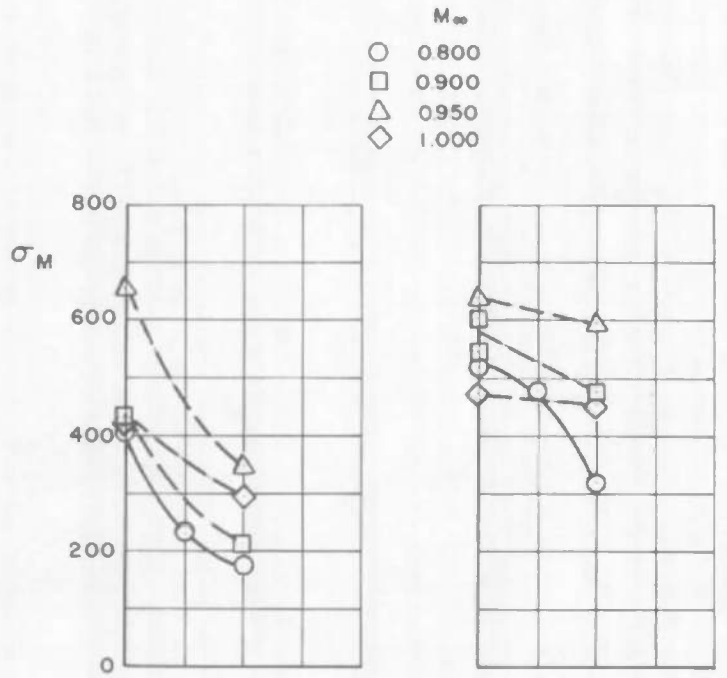

c. Configuration 32

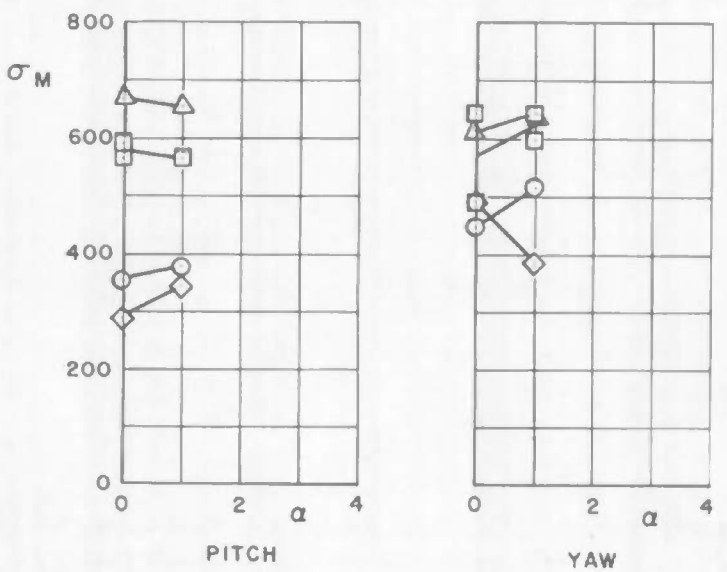

d. Configuration 41

Fig. 23 Continued

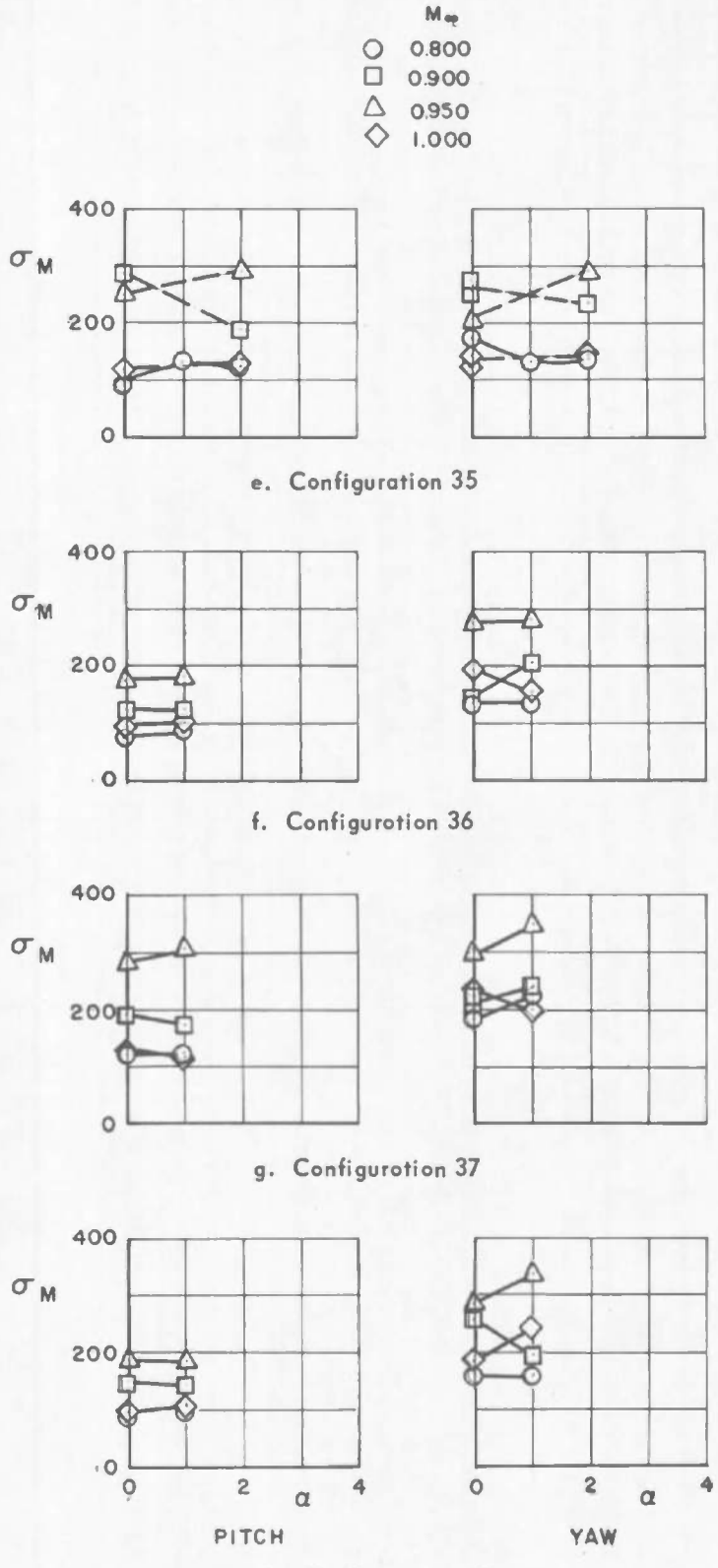

e. Configuration 35

f. Configuration 36

g. Configuration 37

h. Configuration 40

Fig. 23 Concluded

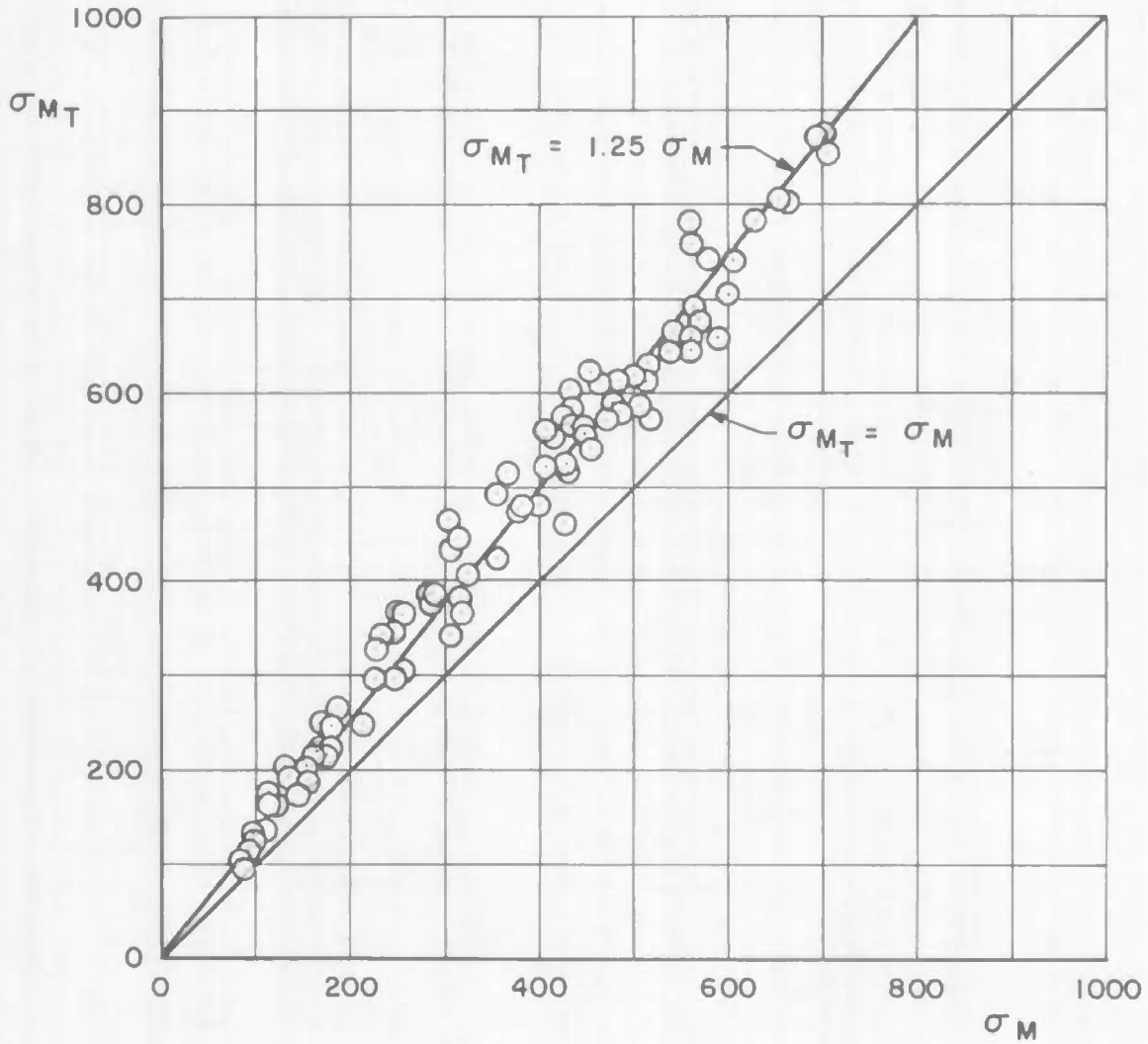

a. Pitch

Fig. 24 Effects of Spring Support System on the RMS Bending Moment

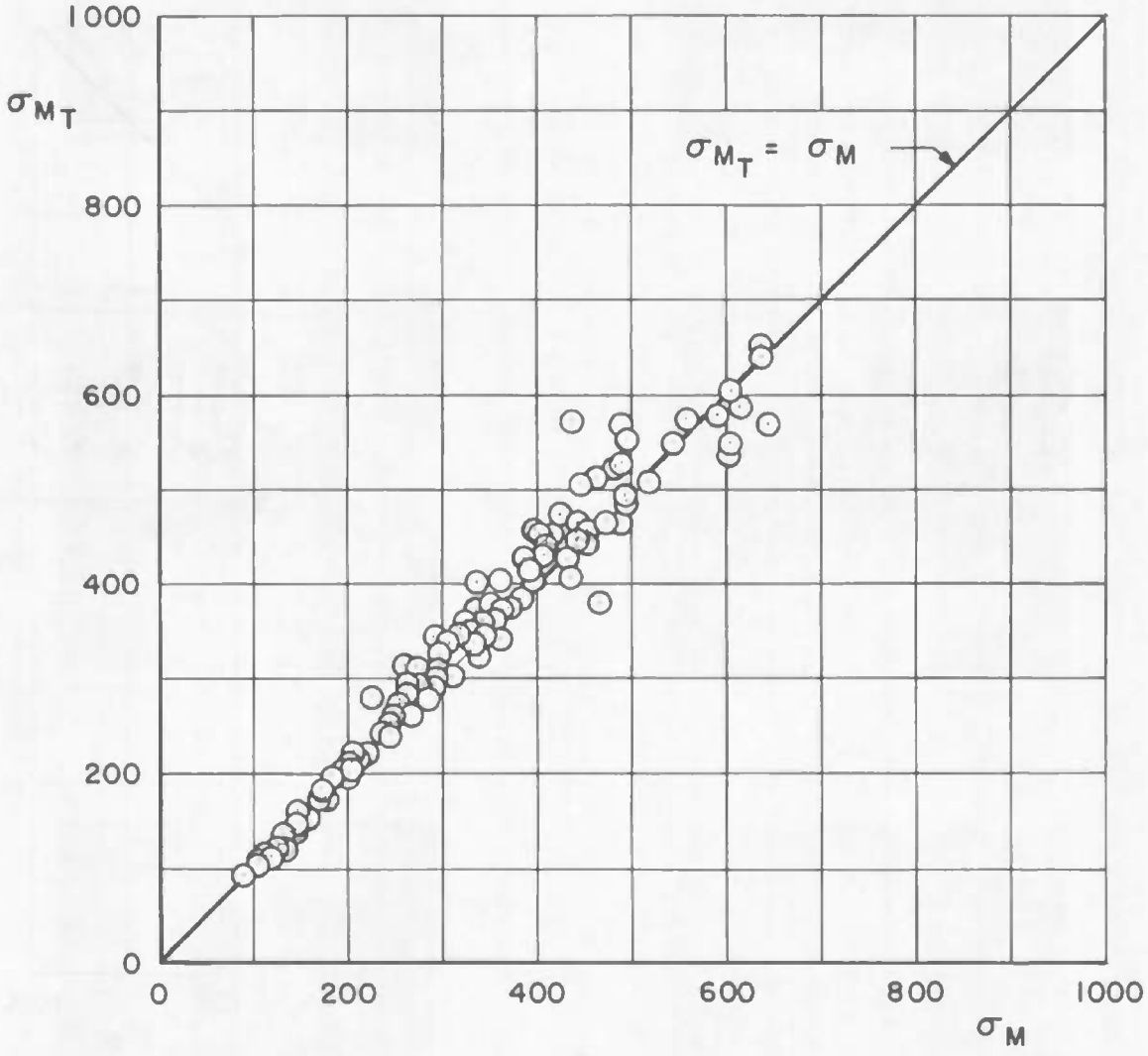

b. Yaw

Fig. 24 Concluded

$M_\infty = 0.70$

$M_\infty = 0.80$

$M_\infty = 0.90$

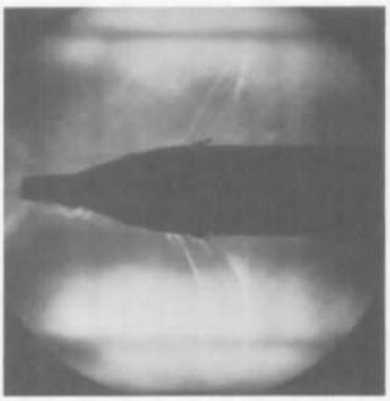

$M_\infty = 0.95$

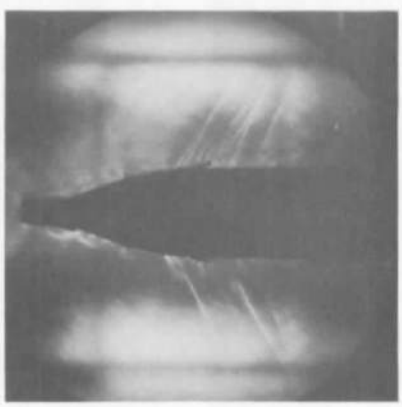

$M_\infty = 1.00$

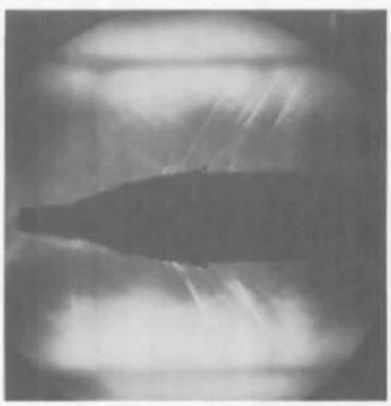

$M_\infty = 1.10$

a. Configuratian 31

Fig. 25 Schlieren Photograph of the Flow about Typical Phase III Test Configurations

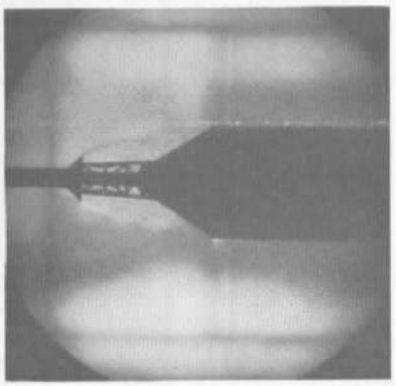

$M_\infty = 0.70$

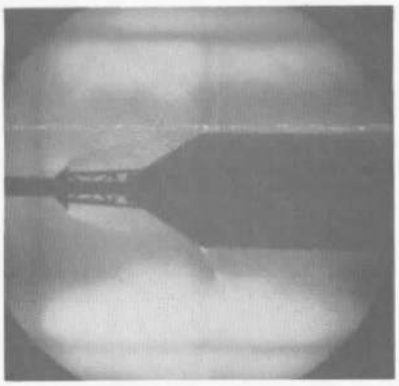

$M_\infty = 0.80$

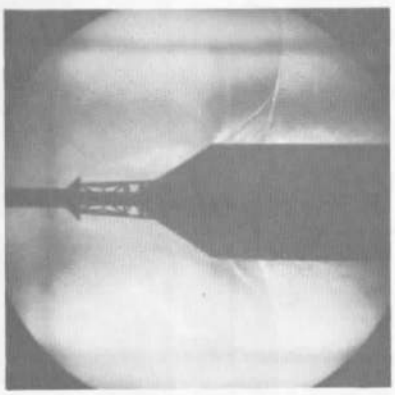

$M_\infty = 0.90$

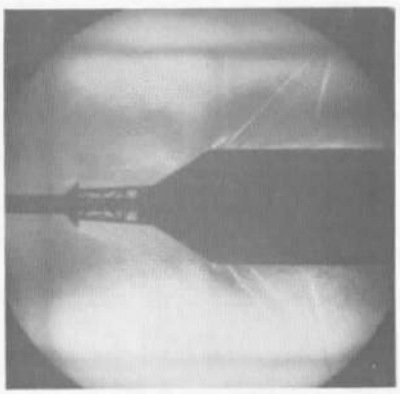

$M_\infty = 0.95$

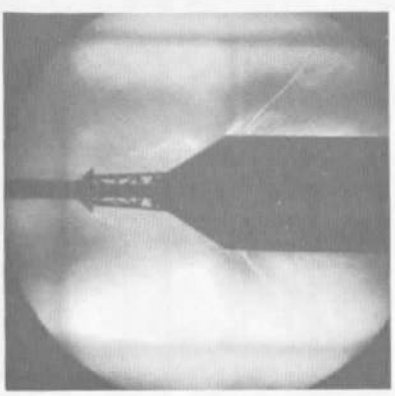

$M_\infty = 1.00$

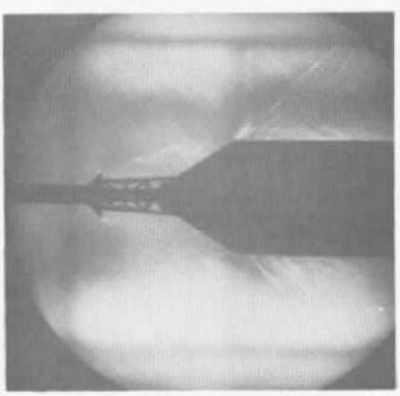

$M_\infty = 1.10$

b. Configuration 37

Fig. 25 Concluded

TABLE I
PHYSICAL PROPERTIES OF TYPICAL PHASE II TEST CONFIGURATIONS

Physical Property		Config. 1		Config. 2		Config. 3		Config. 5		Config. 8		Config. 9		Config. 20	
		Free-Free Bending Modes													
		Pitch	Yaw	Pitch	Yaw	Pitch	Yaw	Pitch	Yaw	Pitch	Yaw	Pitch	Yaw	Pitch	Yaw
f_1	a	45.4	---	24.3	23.3	19.9	19.0	19.0	18.7	22.7	20.0	19.7	19.0	20.6	20.0
	b	43.1	43.1	23.2	20.5	21.0	18.9	21.0	18.9	23.9	19.4	18.5	17.1	---	---
f_2	a	97.8	---	40.0	49.1	40.0	42.2	40.5	42.5	32.8	36.3	39.9	42.3	40.2	40.4
	b	87.0	87.0	40.2	39.6	38.0	38.5	38.0	38.5	39.7	40.2	38.2	35.5	---	---
f_3	a	192.4	---	76.8	100.2	60.3	72.7	52.2	73.0	59.1	53.5	57.1	76.5	67.9	50.8
	b	188.1	188.1	71.6	79.7	61.1	54.7	61.1	54.7	76.78	49.5	57.1	51.7	---	---
$\left(\frac{C_s + C_c}{C_{cr}}\right)_1$	a	0.006	---	0.014	0.025	0.0295	0.020	0.008	0.018	0.056	0.011	0.028	0.025	0.031	0.044
	b	0.020	0.020	0.045	0.045	0.045	0.045	0.045	0.045	0.045	0.045	0.045	0.045	0.045	0.045
W	a	87.75		394.6		411.0		404.5		475.3		398.4		388.6	
	b	87.74		376.4		386.4		---		460.2		378.4		---	

Where: (1) Subscripts 1, 2, and 3 denote first, second, and third bending modes, respectively.
(2) a and b denote actual and design values, respectively.
(3) C_{cr} denotes critical damping.
(4) Weight represents $M_\infty = 1.0$ condition.

TABLE II
PHYSICAL PROPERTIES OF TYPICAL PHASE III TEST CONFIGURATIONS

Physical Property		Config. 30		Config. 31		Config. 32		Config. 34		Config. 36		Config. 37		Config. 41	
		Free-Free Bending Modes													
		Pitch	Yaw	Pitch	Yaw	Pitch	Yaw	Pitch	Yaw	Pitch	Yaw	Pitch	Yaw	Pitch	Yaw
f_1	a	24.8	21.0	18.5	16.7	19.5	18.7	16.5	15.7	19.2	18.7	17.3	16.5	16.5	17.6
	b	---	---	16.0	13.9	18.2	15.3	14.8	13.1	15.3	13.4	15.1	13.6	16.0	13.9
f_2	a	41.5	45.2	31.5	27.0	31.6	30.3	29.6	27.3	30.1	29.0	30.4	29.2	28.7	30.0
	b	---	---	28.6	27.4	30.2	29.6	27.8	26.6	25.7	24.5	24.2	23.8	28.6	27.4
f_3	a	83.0	96.0	80.5	95.0	83.0	94.0	79.0	87.0	79.9	80.0	68.0	77.0	95.0	82.0
	b	---	---	76.9	86.7	72.7	86.8	70.6	82.7	38.2	63.3	49.4	60.4	76.9	86.7
$\left(\frac{C_s + C_c}{C_{cr}}\right)_1$	a	0.024	0.015	0.032	0.024	0.023	0.027	0.015	0.014	0.020	0.019	0.021	0.016	0.016	0.018
	b	0.035	0.035	0.035	0.035	0.035	0.035	0.035	0.035	0.035	0.035	0.035	0.035	0.035	0.035
W	a	471.7		471.2		470.3		472.8		471.4		469.9		471.2	
	b	457.4		456.4		454.5		456.3		455.4		456.9		456.4	

Where: (1) Subscripts 1, 2, and 3 denote first, second, and third bending modes, respectively.
(2) a and b denote actual and design values, respectively.
(3) C_{cr} denotes critical damping.
(4) Weight represents M_∞ = 1.0 condition.

APPENDIX II
MODEL SCALING

The models were aeroelastically scaled to be dynamically similar to the prototype vehicles. The scale factors used in the model design were dictated by the wind tunnel size and the necessity to match pertinent dimensionless and independent parameters [referred to as pi (π) terms, Ref. 3]. The descriptive variables and the basic dimensions are:

Symbol	Variable	Dimensions
a_∞	Free-stream speed of sound	LT^{-1}
E	Young's modulus of elasticity	FL^{-2}
f	Frequency	T^{-1}
g	Gravitational acceleration	LT^{-2}
I_a	Area moment of inertia	L^4
I_m	Mass moment of inertia	FT^2L
ℓ	Typical linear dimension	L
M	Total mass	FT^2L^{-1}
m	Mass per unit length	FT^2L^{-2}
T_∞	Free-stream temperature	θ
V_∞	Free-stream velocity	LT^{-1}
α	Angle of attack	Dimensionless
ν_∞	Kinematic viscosity of the free stream	L^2T^{-1}
ρ_a	Mass density of air	FT^2L^{-4}
ρ_s	Mass density of structure	FT^2L^{-4}

where L, T, F, and θ are the basic dimensions of length, time, force, and temperature, respectively.

The following design conditions were considered pertinent:

$$\left(\frac{\ell}{\ell_{ref}}\right)_M = \left(\frac{\ell}{\ell_{ref}}\right)_P \quad \text{(Geometry)} \tag{1}$$

$$\left(\frac{V_\infty}{a_\infty}\right)_M = \left(\frac{V_\infty}{a_\infty}\right)_P \quad \text{(Mach number)} \tag{2}$$

$$\left(\frac{f\ell}{V_\infty}\right)_M = \left(\frac{f\ell}{V_\infty}\right)_P \quad \text{(Strouhal number)} \tag{3}$$

$$\alpha_M = \alpha_P \quad \text{(Angle of attack)} \tag{4}$$

$$\left(\frac{\rho_a}{\rho_s}\right)_M = \left(\frac{\rho_a}{\rho_s}\right)_P \quad \text{(Mass density ratio)} \tag{5}$$

where M and P denote model and prototype, respectively, and ref denotes a reference parameter. To satisfy tunnel requirements for less than one-percent tunnel blockage, $(\ell_{ref})_M = 0.07\ (\ell_{ref})_P$.

From the necessity to match Mach number, Eq. (2), it can be shown that

$$\frac{(V_\infty)_M}{(V_\infty)_P} = \left[(T_\infty)_M/(T_\infty)_P\right]^{1/2} \tag{6}$$

where T_∞ is absolute temperature in degrees Rankine. Because of limitations in the test facility, there was a temperature mismatch between the model test conditions and the prototype flight regimes.

This mismatch is considered small, such that $\frac{(V_\infty)_M}{(V_\infty)_P} \approx 1.0$.

The bending stiffness and running mass of the model were also the correct scaled values of the prototype vehicle.

$$\left(\frac{EI_a}{EI_{a_{ref}}}\right)_M = \left(\frac{EI_a}{EI_{a_{ref}}}\right)_P \tag{7}$$

$$\left(\frac{m}{m_{ref}}\right)_M = \left(\frac{m}{m_{ref}}\right)_P \tag{8}$$

The necessity to match pertinent conditions Eqs. (1) through (6) resulted in a mismatch in certain remaining π terms.

For example:

$$\left(\frac{V_\infty \ell}{\nu_\infty}\right)_M = \left(\frac{V_\infty \ell}{\nu_\infty}\right)_P \quad \text{(Reynolds number)} \tag{9}$$

and

$$\left(\frac{V_\infty^2}{g\ell}\right)_M = \left(\frac{V_\infty^2}{g\ell}\right)_P \quad \text{(Froude number)} \tag{10}$$

The mismatch in Reynolds number implies a lack of similarity in the boundary layers on the model and prototype vehicles. The mismatch in Froude number implies a lack of similarity in the gravity effects or that slosh and "deadweight" are not matched. It was felt that these mismatched conditions were not critical to the nature of the test.

The various parameters of the model are defined as follow:

Scale Factor	$n = 0.07$
Length	$\frac{\ell_M}{\ell_P} = n = 0.07$
Stiffness	$\frac{(EI_s)_M}{(EI_s)_P} = (n)^4 = 2.40 \times 10^{-3}$
Mass	$\frac{M_M}{M_P} = (n)^3 = 3.43 \times 10^{-4}$
Running Mass	$\frac{m_M}{m_P} = (n)^2 = 4.90 \times 10^{-3}$
Frequency	$\frac{f_M}{f_P} = \frac{1}{n} = 14.28$
Mass Moment of Inertia	$\frac{(I_m)_M}{(I_m)_P} = (n)^5 = 1.68 \times 10^{-6}$

Security Classification

DOCUMENT CONTROL DATA - R&D

(Security classification of title, body of abstract and indexing annotation must be entered when the overall report is classified)

1 ORIGINATING ACTIVITY (Corporate author) Arnold Engineering Development Center ARO, Inc., Operating Contractor Arnold Air Force Station, Tennessee	2a REPORT SECURITY CLASSIFICATION UNCLASSIFIED 2b GROUP N/A

3 REPORT TITLE

BUFFET RESPONSE OF AEROELASTICALLY SCALED TITAN III MISSILE CONFIGURATIONS AT TRANSONIC MACH NUMBERS

4 DESCRIPTIVE NOTES (Type of report and inclusive dates)

N/A

5 AUTHOR(S) (Last name, first name, initial)

Robertson, J. E. and Brice, T. R., ARO, Inc.

6 REPORT DATE	7a TOTAL NO OF PAGES	7b NO OF REFS
March 1967	78	4

8a CONTRACT OR GRANT NO AF 40(600)-1200 b PROJECT NO. Program Element 64409094/624A c d	9a ORIGINATOR'S REPORT NUMBER(S) AEDC-TR-67-33 9b OTHER REPORT NO(S) (Any other numbers that may be assigned this report) N/A

10 AVAILABILITY/LIMITATION NOTICES

This document is subject to special export controls and each transmittal to foreign governments or foreign nationals may be made only with prior approval of Space Systems Division (SSBDD), Los Angeles, California.

11 SUPPLEMENTARY NOTES	12 SPONSORING MILITARY ACTIVITY
Available in DDC	Space Systems Division Air Force Systems Command Los Angeles, California

13 ABSTRACT A wind tunnel investigation was conducted to obtain the structural response of 0.07-scaled aeroelastic models of Titan III missile configurations to buffet airloads at transonic Mach numbers. Test results in the form of bending-moment response in the pitch and yaw planes were obtained for various payload, upper stage, and booster combinations. The tests were conducted in the Mach number range from 0.6 to 1.4 and at angles of attack ranging from 0 to 4 deg. The basic Centaur/Voyager configuration experienced flutter in the first pitch and yaw elastic bending modes as Mach number was increased above 0.80. The flutter was eliminated by (1) adding to the payload a cylindrical shroud having the same diameter as the payload and (2) adding to the payload a boattail shroud with a ring of vortex generators upstream of the boattail. The MOL and Apollo configurations exhibited slightly different trends in the bending-moment variations with Mach number, although both configuration families experienced peak loads at Mach numbers near 0.95. Increasing dynamic pressure caused a proportionate increase in the pitch and yaw structural response. Increasing angle of attack, in general, resulted in a reduction in the structural response, although there were deviations from this trend for certain configurations.

DD FORM 1 JAN 64 1473

Security Classification

14 KEY WORDS	LINK A ROLE	LINK A WT	LINK B ROLE	LINK B WT	LINK C ROLE	LINK C WT
Titan III						
transonic flow						
buffeting						
turbulence						
structural integrity						
aeroelastic model						
bending modes						
1. missiles -- Titan III						
3. " -- Buffeting						
4. Space vehicles -- " "						

INSTRUCTIONS

1. ORIGINATING ACTIVITY: Enter the name and address of the contractor, subcontractor, grantee, Department of Defense activity or other organization *(corporate author)* issuing the report.

2a. REPORT SECURITY CLASSIFICATION: Enter the overall security classification of the report. Indicate whether "Restricted Data" is included. Marking is to be in accordance with appropriate security regulations.

2b. GROUP: Automatic downgrading is specified in DoD Directive 5200.10 and Armed Forces Industrial Manual. Enter the group number. Also, when applicable, show that optional markings have been used for Group 3 and Group 4 as authorized

3. REPORT TITLE: Enter the complete report title in all capital letters. Titles in all cases should be unclassified. If a meaningful title cannot be selected without classification, show title classification in all capitals in parenthesis immediately following the title.

4. DESCRIPTIVE NOTES: If appropriate, enter the type of report, e.g., interim, progress, summary, annual, or final. Give the inclusive dates when a specific reporting period is covered.

5. AUTHOR(S): Enter the name(s) of author(s) as shown on or in the report. Enter last name, first name, middle initial. If military, show rank and branch of service. The name of the principal author is an absolute minimum requirement.

6. REPORT DATE: Enter the date of the report as day, month, year, or month, year. If more than one date appears on the report, use date of publication.

7a. TOTAL NUMBER OF PAGES: The total page count should follow normal pagination procedures, i.e., enter the number of pages containing information.

7b. NUMBER OF REFERENCES: Enter the total number of references cited in the report.

8a. CONTRACT OR GRANT NUMBER: If appropriate, enter the applicable number of the contract or grant under which the report was written.

8b, 8c, & 8d. PROJECT NUMBER: Enter the appropriate military department identification, such as project number, subproject number, system numbers, task number, etc.

9a. ORIGINATOR'S REPORT NUMBER(S): Enter the official report number by which the document will be identified and controlled by the originating activity. This number must be unique to this report.

9b OTHER REPORT NUMBER(S): If the report has been assigned any other report numbers *(either by the originator or by the sponsor)*, also enter this number(s).

10. AVAILABILITY/LIMITATION NOTICES: Enter any limitations on further dissemination of the report, other than those imposed by security classification, using standard statements such as:

(1) "Qualified requesters may obtain copies of this report from DDC."

(2) "Foreign announcement and dissemination of this report by DDC is not authorized."

(3) "U. S. Government agencies may obtain copies of this report directly from DDC. Other qualified DDC users shall request through

_____."

(4) "U. S. military agencies may obtain copies of this report directly from DDC. Other qualified users shall request through

_____."

(5) "All distribution of this report is controlled. Qualified DDC users shall request through

_____."

If the report has been furnished to the Office of Technical Services, Department of Commerce, for sale to the public, indicate this fact and enter the price, if known.

11. SUPPLEMENTARY NOTES: Use for additional explanatory notes.

12. SPONSORING MILITARY ACTIVITY: Enter the name of the departmental project office or laboratory sponsoring *(paying for)* the research and development. Include address.

13. ABSTRACT: Enter an abstract giving a brief and factual summary of the document indicative of the report, even though it may also appear elsewhere in the body of the technical report. If additional space is required, a continuation sheet shall be attached.

It is highly desirable that the abstract of classified reports be unclassified. Each paragraph of the abstract shall end with an indication of the military security classification of the information in the paragraph, represented as *(TS)*, *(S)*, *(C)*, or *(U)*

There is no limitation on the length of the abstract. However, the suggested length is from 150 to 225 words.

14. KEY WORDS: Key words are technically meaningful terms or short phrases that characterize a report and may be used as index entries for cataloging the report. Key words must be selected so that no security classification is required. Identifiers, such as equipment model designation, trade name, military project code name, geographic location, may be used as key words but will be followed by an indication of technical context. The assignment of links, rules, and weights is optional.